


Investigation of approximate mode shape and transition velocity of pipe conveying fluid in failure analysis

Advances in Mechanical Engineering
2022, Vol. 14(1) 1–24
© The Author(s) 2022
DOI: 10.1177/16878140211072410
journals.sagepub.com/home/ade


Wasiu Adeyemi Oke¹ , Oluseyi Afolabi Adeyemi² and Ayodeji Olalekan Salau³

Abstract

Structures dynamic characteristics and their responses can change due to variations in system parameters. With modal characteristics of the structures, their dynamic responses can be identified. Mode shape remains vital in dynamic analysis of the structures. It can be utilized in failure analysis, and the dynamic interaction between structures and their supports to circumvent abrupt failure. Conversely, unlike empty pipes, the mode shapes for pipes conveying fluid are tough to obtain due to the intricacy of the eigenvectors. Unfortunately, fluid pipes can be found in practice in various engineering applications. Thus, due to their global functions, their dynamic and failure analyses are necessary for monitoring their reliability to avert catastrophic failures. In this work, three techniques for obtaining approximate mode shapes (AMSs) of composite pipes conveying fluid, their transition velocity and relevance in failure analysis were investigated. Hamilton's principle was employed to model the pipe and discretized using the wavelet-based finite element method. The complex modal characteristics of the composite pipe conveying fluid were obtained by solving the generalized eigenvalue problem and the mode shapes needed for failure analysis were computed. The proposed methods were validated, applied to failure analysis, and some vital results were presented to highlight their effectiveness.

Keywords

Composite pipe conveying fluid, mode shapes, complex eigenvectors, wavelets, failure

Date received: 17 September 2021; accepted: 17 December 2021

Handling Editor: Chenhui Liang

Introduction

Indeed, the involvement of pipes for conveying fluid is increasing on a daily basis and there is no sign that the trend will cease or decline in the nearest future. This is due to the frequent use of pipes for conveying fluid in oil and water pipelines, marine risers, chemical plants, nuclear industry, aerospace, irrigation, and municipality just to mention a few. These pipes are subjected to flow-induced vibration during the operation as a result of turbulence in the flow and this may easily cause pipe failures. Thus, dynamic analysis of the pipes conveying fluid is necessary for monitoring the pipes integrity to avoid failure. Many investigators have worked on pipe

failure analysis using different techniques. Bhardwaj et al.¹ examined the reliability of the structure of a

¹Department of Mechanical and Mechatronics Engineering, Afe Babalola University, Ado-Ekiti, Nigeria

²Department of Mechanical Engineering, First Technical University, Ibadan, Nigeria

³Department of Electrical/Electronics and Computer Engineering, Afe Babalola University, Ado-Ekiti, Nigeria

Corresponding author:

Wasiu Adeyemi Oke, Department of Mechanical and Mechatronics Engineering, College of Engineering, Afe Babalola University, P.M.B 5454, Ado-Ekiti, Ekiti 360231, Nigeria.
Email: wasiuad@abuad.edu.ng



pipe-in-pipe in deep-waters under critical operating conditions. In their study, the First-Order and Second-Order, reliability techniques, and Monte Carlo Simulation methods were employed. Chu et al.² analyzed the failure of a steam pipe that has been in service for more than one decade. Finite element analysis and experimental methods were considered during the analysis. Majid et al.³ carried out the failure analysis of eroded pipe using the computational fluid dynamics and experimental methods. Some researchers have also made use of machine learning and dynamic analysis in the pipe failures analysis. For instance, Tang et al.⁴ investigated the plastic water pipe failure using Bayesian network models in which a guided method and automated learning algorithms were employed. Also, Robles-Velasco et al.⁵ employed support vector classification and logistic regression as predictive systems to predict water pipe failures. Ashrafizadeh et al.⁶ studied the crack failure of a gas pipe that has been in service for roughly three decades. In their investigation, dynamic analysis, first mode shape, and others were considered. El-Gebeily et al.⁷ developed a method for detecting pipe internal damage in which vibration modal characteristics were employed and B-spline scaling function was used to formulate the model. Other investigations that have been carried out on pipes failure analysis can be found in Ying et al.,⁸ Rezaei et al.⁹

It can be observed in the above review that pipe mode shapes have not been given much attention in the failure analysis. However, with proper monitoring of the pipe system, any pipe that has been compromised due to internal damage, erosion or chemical attack, and other factors can be detected through the mode shapes. Since geometry can affect mode shapes, monitoring mode shapes can be employed to avoid failure due to the fact that a compromised pipe will display abnormal mode shapes. As a result the majority if not all the failure types or modes observed or mentioned in the review may be avoided. Nevertheless, unlike empty pipes, dynamic analysis of the fluid pipes is difficult because the undamped pipe will become damped as fluid starts flowing through it. Consequently, complex eigenvalues and eigenvectors will emerge and mode shapes constructions become complicated. A suitable technique needs to be employed to be able to obtain mode shapes that can be used in failure analysis, damage assessment, shape estimation, and in order to avoid pessimistic effects of vibration. While significant attentions have been given to the techniques that can be employed to obtain mode shapes of other structures,¹⁰⁻¹⁶ few researchers have paid attentions to the methods for obtaining the mode shapes of pipes conveying fluid. Liu et al.¹⁷ utilized frequency response function based technique to compute mode shapes of fluid pipe while natural frequencies were obtained using a hybrid

analytical numerical technique based on the Transfer Matrix Method. Yun-dong and Yi-ren¹⁸ investigated the free vibration analysis of a pipe conveying fluid with different boundary conditions using He's variational iteration technique and the real part of complex modes was employed to obtain mode shapes. Mediano-Valiente and Garcia Planas¹⁹ studied the dynamics and stability of clamped-pinned pipes conveying fluid using eigenvalues of a Hamiltonian linear system and the natural frequencies and mode shapes employed in their study were also obtained using ANSYS. Arjmandi and Lotfi²⁰ obtained the mode shapes of fluid-structure systems using an accelerated pseudo symmetric subspace iteration method in conjunction with finite element program developed for dynamic analysis of systems. Ryu et al.²¹ employed the concept of quasi-mode shape to examine unstable modal shapes associated with flutter of viscoelastic cantilevered pipes conveying fluid wherein extended Hamilton's principle was used to obtain equation of motion. Wang et al.²² investigated the mode shapes of cantilevered pipes conveying fluid at different flow velocity in which equation of motion was solved using Differential Quadrature Method. Zhou et al.²³ studied the mode shapes of axially functionally graded cantilevered pipes conveying fluid. Their governing equations and the equations for boundary conditions were also discretized using Differential Quadrature Method. Sarkar and Paidoussis²⁴ utilized semi-analytical approach to obtain the proper orthogonal modes of non-linear oscillation of a cantilevered pipe with end-mass conveying fluid.

Regarding marine risers used widely for conveying fluid, Alfossail et al.²⁵ have obtained the natural frequencies and mode shapes of a marine riser using Galerkin approach in which Euler-Bernoulli beam theory was employed to model the riser. Chen et al.²⁶ utilized differential transformation method to study natural frequencies and mode shapes of marine risers with different boundary conditions.

From the review, one can infer that more needs to be done on the construction of mode shapes of structures or pipes conveying fluid in order to be able to use them to examine the integrity of the pipes regularly to avoid plant down time, revenue loss, and catastrophic failure. The work presented in Oke et al.²⁷ was expanded in this study, more AMSs were presented for different pipes at different velocities, and these mode shapes were used to investigate fluid pipe failure analysis. Hamilton's principle was utilized to obtain the equation of motion of the composite pipe conveying fluid. The equation was discretized using the wavelet-based finite element method in which Euler-Bernoulli beam theory was employed. The equation obtained was then expressed in state space to obtain the generalized eigenvalue problem. The AMSs used for failure analysis were then

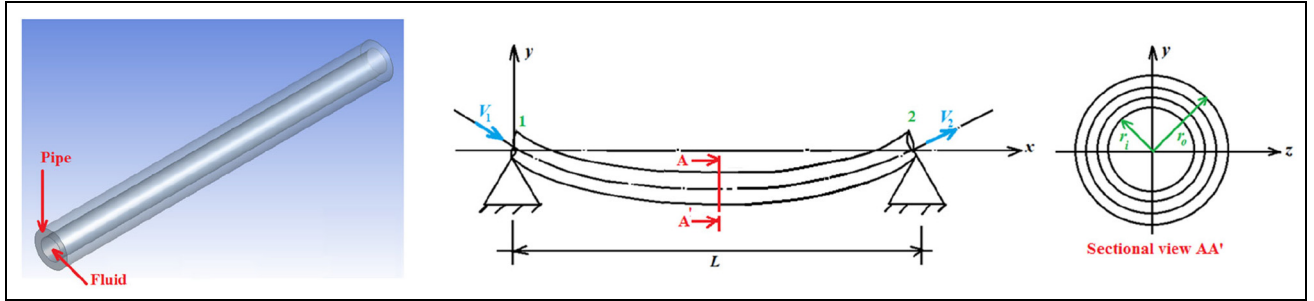


Figure 1. Laminated composite pipe conveying fluid.

constructed from the complex modal characteristics obtained for composite pipe conveying fluid by solving the generalized eigenvalue problem.

Composite pipe conveying fluid system formulation

As the fluid flows through the pipe (see Figure 1) with inlet velocity v_1 and outlet velocity v_2 , the fluid pipe interaction will affect the system vibrational behavior and may lead to failure. The strain energy U of the laminated composite pipe element conveying fluid and the total kinetic energy T (which is the summation of kinetic energy of the composite pipe element and the kinetic energy of the fluid element) can be expressed as

$$U = \frac{1}{2} \int_0^{l_e} \mathcal{H}(x) \left(\frac{\partial^2 y}{\partial x^2} \right)^2 dx, \quad (1)$$

$$T = \frac{1}{2} \int_0^{l_e} \mathcal{M}(x) V_p^2 dx + \frac{1}{2} \int_0^{l_e} m_f V_f^2 dx, \quad (2)$$

where

$$\mathcal{M}(x) = \iint_{A_p} \rho_p dA_p = \sum_{\ell=1}^N \pi \rho_\ell (r_\ell^2 - r_{\ell-1}^2) \text{ kg/m},$$

$$V_f = (\partial y / \partial t) + V \partial y / \partial x, \quad V_p = \partial y / \partial t,$$

$$A_p = 0.25\pi(D_o^2 - D_i^2), \quad A_f = 0.25\pi D_i^2, \quad m_f = \rho_f A_f,$$

in which \mathcal{H} and \mathcal{M} are stiffness and mass per unit length of the laminated composite pipe element; D_o and D_i are pipe outer and inner diameters; and r_ℓ and ρ_ℓ are radius and density of ℓ^{th} layer. Besides, with stiffness coefficients A_{11} , B_{11} , and D_{11} , an equation utilized in Oke and Khulief²⁸ can be defined for healthy composite pipe conveying fluid shown in Figure 1 as

$$\mathcal{H} = \pi R^3 (A_{11} + 2B_{11}/R + D_{11}/R^2), \quad (3)$$

where $R = (D_i + D_o)/4$.

Equation of motion of composite pipe conveying fluid

The Hamilton's principle can be defined as

$$\int_{t_1}^{t_2} (\delta U - \delta T) dt = 0. \quad (5)$$

By substituting equations (1) and (2) in equation (5), it gives

$$\int_{t_1}^{t_2} \left\{ \left[\int_0^{l_e} \mathcal{H}(x) \frac{\partial^4 y}{\partial x^4} \delta y dx \right] - \left[\delta \left(\frac{1}{2} \int_0^{l_e} m_e \left(\frac{\partial y}{\partial t} \right)^2 dx \right) + \delta \left(\frac{1}{2} \int_0^{l_e} 2m_f V \frac{\partial^2 y}{\partial t \partial x} dx \right) - \int_0^{l_e} m_f V^2 \frac{\partial^2 y}{\partial x^2} \delta y dx \right] \right\} dt = 0. \quad (6)$$

Then, equation of motion for the laminated composite pipe with fluid flow can be obtained through the simplification of equation (6) as

$$\mathcal{H}(x) \frac{\partial^4 y}{\partial x^4} + m_e \frac{\partial^2 y}{\partial t^2} + m_f V \left(2 \frac{\partial^2 y}{\partial t \partial x} + V \frac{\partial^2 y}{\partial x^2} \right) = 0, \quad (7)$$

where $m_e = \mathcal{M}(x) + m_f$. It should be noted that equation (7) contains four major terms: the pipe stiffness, pipe inertia, Coriolis force, and centrifugal force that arises due to fluid acceleration through the distorted pipe curvature.

The finite element formulation of composite pipe conveying fluid

Using the Euler-Bernoulli pipe element, equation (7) has been discretized in order to solve it, wherein the B-spline wavelet on the interval was used as it was in Oke and Khulief.²⁸ As a result, equation (7) can be stated in a condensed form as

Table 1. Composite pipes properties.

Property	Pipe P_1 ^{27,30–32}	Pipe P_2 ^{28,31,32}	Pipe P_3
D_o	0.1282 m	0.1126 m	0.1282 m
D_i	0.1256 m	0.1016 m	0.1256 m
Ply angles/stacking sequence (°)	[90/45/–45/0 _g /90] (inner to outer layers)	[± 54 _s /54] (inner to outer layers)	[0/± 45/0/45/0/45/0/± 45] (inner to outer layers)
Length of pipe, L	2.470 m	2.00 m	3.00 m
E_{11}	211 GPa	12.5 GPa	211 GPa
E_{22}	24.1 GPa	7.1429 GPa	24.1 GPa
$G_{12} = G_{13} = G_{23}$	6.9 GPa	3.3194 GPa	6.9 GPa
Poisson ratio, ν_{12}	0.36	0.56	0.36
Density, ρ	1967 kg/m ³	1730 kg/m ³	1967 kg/m ³

$$[M]_e \{\ddot{y}\}_e + [B]_e \{\dot{y}\}_e + [K]_e \{y\}_e = \{0\}, \quad (8)$$

where

$$\begin{aligned} [M]_e &= \int_0^{l_e} l_e m_e [T_B]^T \{\Psi\}^T \{\Psi\} [T_B] d\zeta, \quad [B]_e \\ &= \int_0^{l_e} 2m_f V [T_B]^T \{\Psi\}^T \{\Psi'\} [T_B] d\zeta, \\ [K]_e &= [K_p]_e - [K_c]_e, \\ [K_p]_e &= \int_0^{l_e} \frac{\mathcal{H}}{l_e^3} [T_B]^T \{\Psi''\}^T \{\Psi''\} [T_B] d\zeta, \text{ and } [K_c]_e \\ &= \int_0^{l_e} \frac{1}{l_e} m_f V^2 [T_B]^T \{\Psi'\}^T \{\Psi'\} [T_B] d\zeta. \end{aligned}$$

Besides, equation (8) can be stated in state space using the state vectors $\{z\}$ and $\{\dot{z}\}$ as

$$[\bar{M}]\{\dot{z}\} - [\bar{K}]\{z\} = \{0\}, \quad (9)$$

where

$$\begin{aligned} [\bar{M}] &= \begin{bmatrix} [I] & [0] \\ [0] & [M]_e \end{bmatrix}, \quad [\bar{K}] = \begin{bmatrix} [0] & [I] \\ -[K]_e & -[B]_e \end{bmatrix}, \\ \{z\} &= \begin{bmatrix} \{y_1\} \\ \{y_2\} \end{bmatrix}, \quad \{\dot{z}\} = \begin{bmatrix} \{\dot{y}_1\} \\ \{\dot{y}_2\} \end{bmatrix}. \end{aligned}$$

These vectors can be expressed for harmonic motion as

$$\{z\} = \{W\}e^{i\omega t}, \quad \{\dot{z}\} = i\omega\{W\}e^{i\omega t}. \quad (10)$$

By substituting equation (10) in equation (9), the generalized eigenvalue problem can be obtained as

$$[[\bar{K}] - \lambda[\bar{M}]]\{W\} = \{0\}, \quad (11)$$

where $\lambda = i\omega$ and ω is frequency.

Now, the dimension of each matrix in equation (8) is $n \times n$ while that of matrix in equation (11) is $2n \times 2n$.

Numerical results and discussion

Here, AMSs of six pinned-pinned pipes (four composite and two isotropic pipes) were examined and subsequent failure analysis of one of them. The results obtained are as follows:

Composite pipes

The composite pipes ($P_1 - P_2$) defined in Table 1 that have been considered by many investigators along with pipe P_3 were considered with fluid flow so as to study their vibration behavior and AMSs. Pipe P_3 uses the stacking sequence given in Bauchau,²⁹ and material and geometric properties of P_1 except length. In order to validate the model, the fundamental frequency of each pipe without fluid flow was firstly obtained and the results obtained are 98.76, 33.42, and 56.48 Hz respectively. These results agreed with those available in literature or aforementioned Refs. for P_1 and P_2 . In addition, the mode shapes for the first four frequencies for these pipes are presented in Figure 2 and it can be seen that they agreed with mode shapes of pinned-pinned structures.

Moreover, each of these pipes was then studied one after the other as the pipe conveying fluid at five different velocities that are less than each pipe critical velocity V_c . The fluid used in this investigation was water with density of 998.2 kg/m³ at all velocities considered. The pipes that were initially undamped suddenly became damped structures as a result of the fluid flowing through them. Consequently, the $2n$ complex conjugate λ and eigenvectors were obtained but these made the mode shapes to become difficult to obtain as in Figure 2. Nevertheless, by using any of the following three methods: real part, imaginary part, and absolute of complex eigenvectors; the AMSs were obtained from complex eigenvectors. The AMSs obtained for the

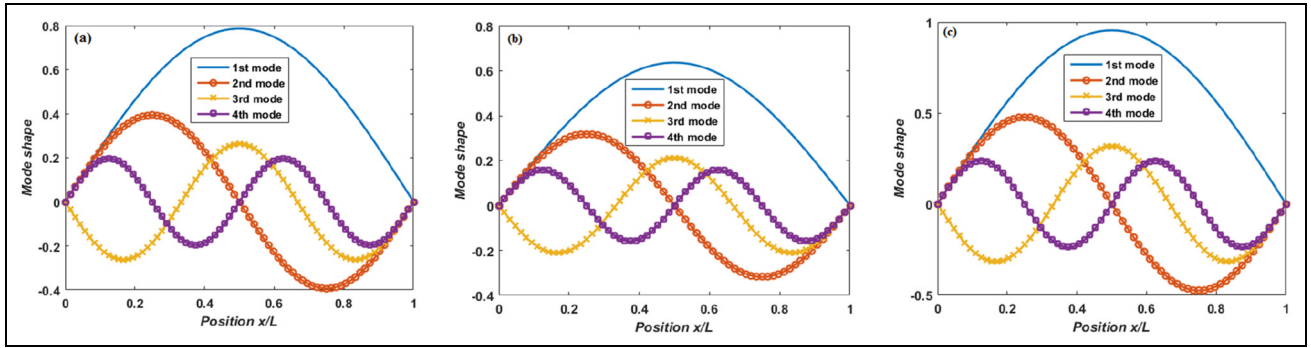


Figure 2. Different pipes mode shapes for the first four frequencies: (a) P_1 , (b) P_2 , and (c) P_3 .

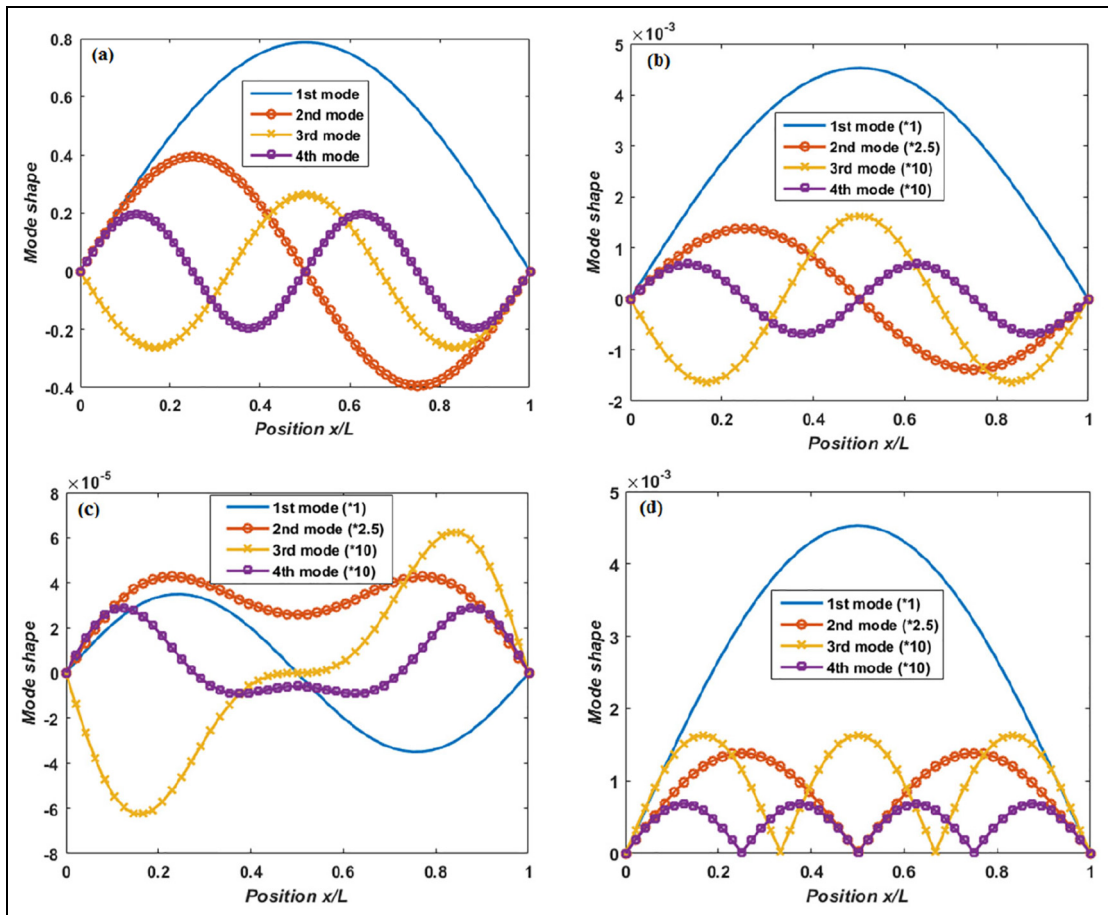


Figure 3. (a) Mode shapes for empty Pipe; (b–d) are imaginary, real, and absolute mode shapes for pipe conveying fluid at $V = 10$ m/s.

pipes conveying fluid (damped pipes) at different velocities are compared with their mode shapes (in Figure 2) when they were empty pipes (undamped pipes). The results obtained are as presented in Figures 3 to 7 for P_1 , Figures 8 to 12 for P_2 , and Figures 13 to 17 for P_3 respectively, where “(a)” in Figures 3 to 7 is the same as Figure 2(a), “(a)” in Figures 8 to 12 is the same as Figure 2(b), and “(a)” in Figures 13 to 17 is the

same as Figure 2(c). It can be found that the mode shapes for the pipes had been reduced generally when compared to those available when they were empty. Besides, at lower velocities, it is fascinating to see that the mode shapes obtained for these pipes from the imaginary part of their complex eigenvectors offered the mode shapes that are similar to pinned-pinned pipes mode shapes (see Figure 2). At the same time, the

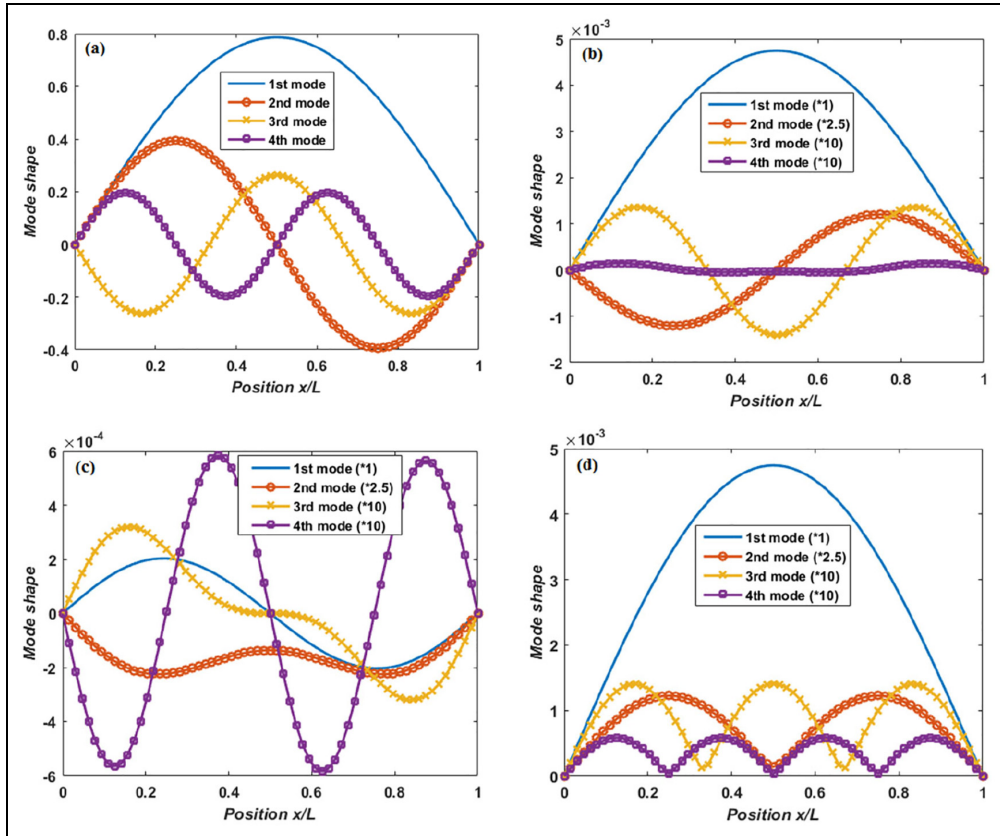


Figure 4. (a) Mode shapes for empty Pipe; (b–d) are imaginary, real, and absolute mode shapes for pipe conveying fluid at $V = 60$ m/s.

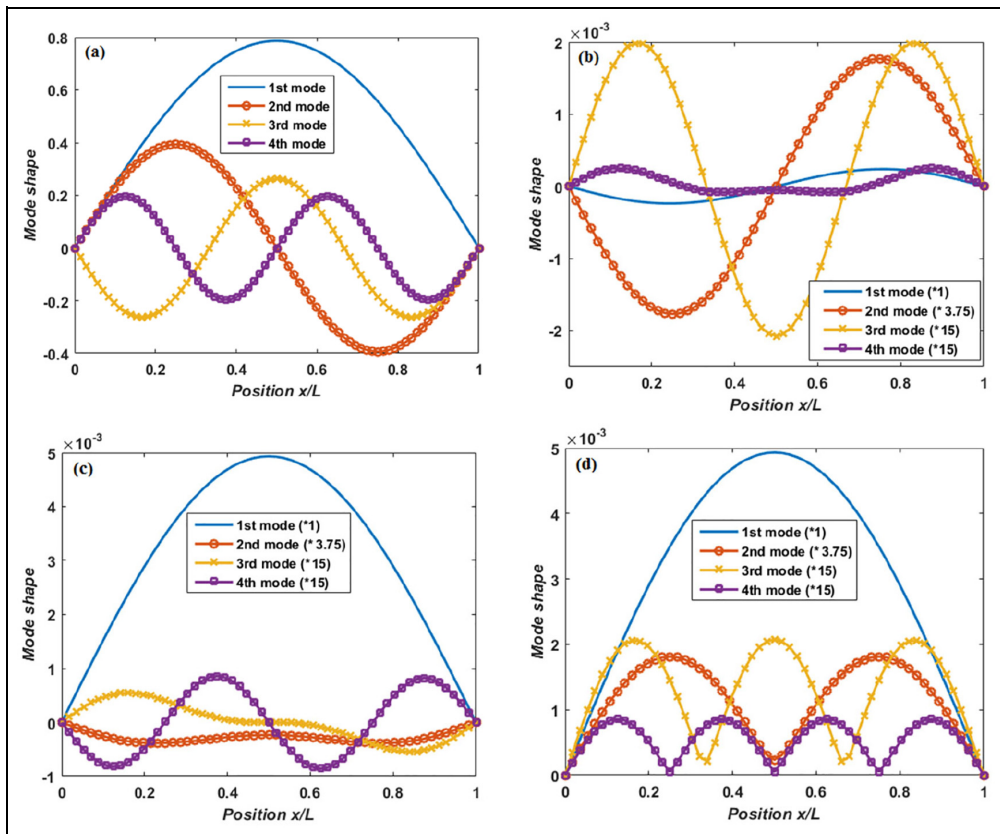


Figure 5. (a) Mode shapes for empty Pipe; (b–d) are imaginary, real, and absolute mode shapes for pipe conveying fluid at $V = 70$ m/s.

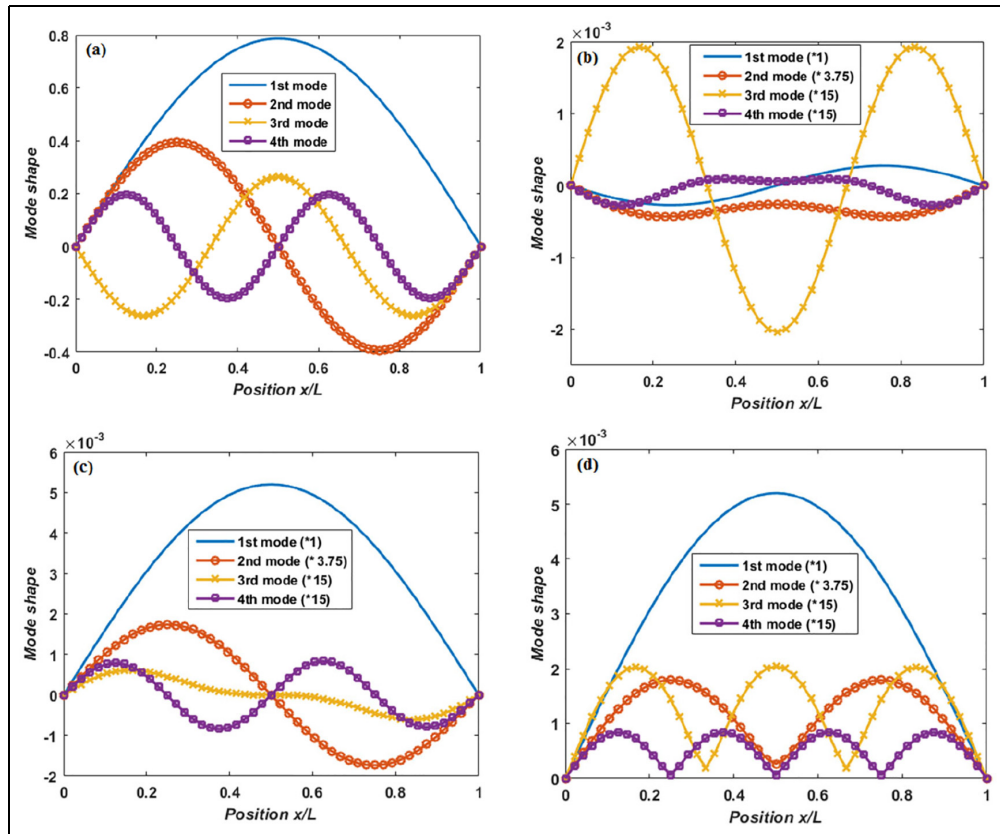


Figure 6. (a) Mode shapes for empty Pipe; (b–d) are imaginary, real, and absolute mode shapes for pipe conveying fluid at $V = 80$ m/s.

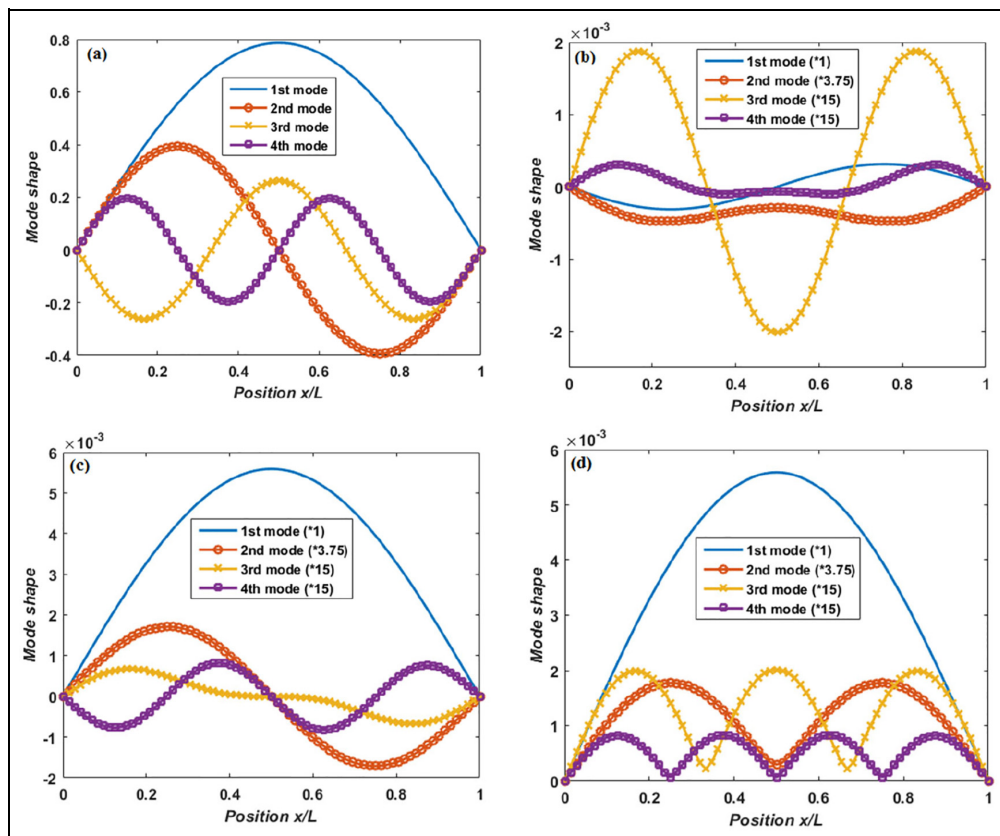


Figure 7. (a) Mode shapes for empty Pipe; (b–d) are imaginary, real, and absolute mode shapes for pipe conveying fluid at $V = 90$ m/s.

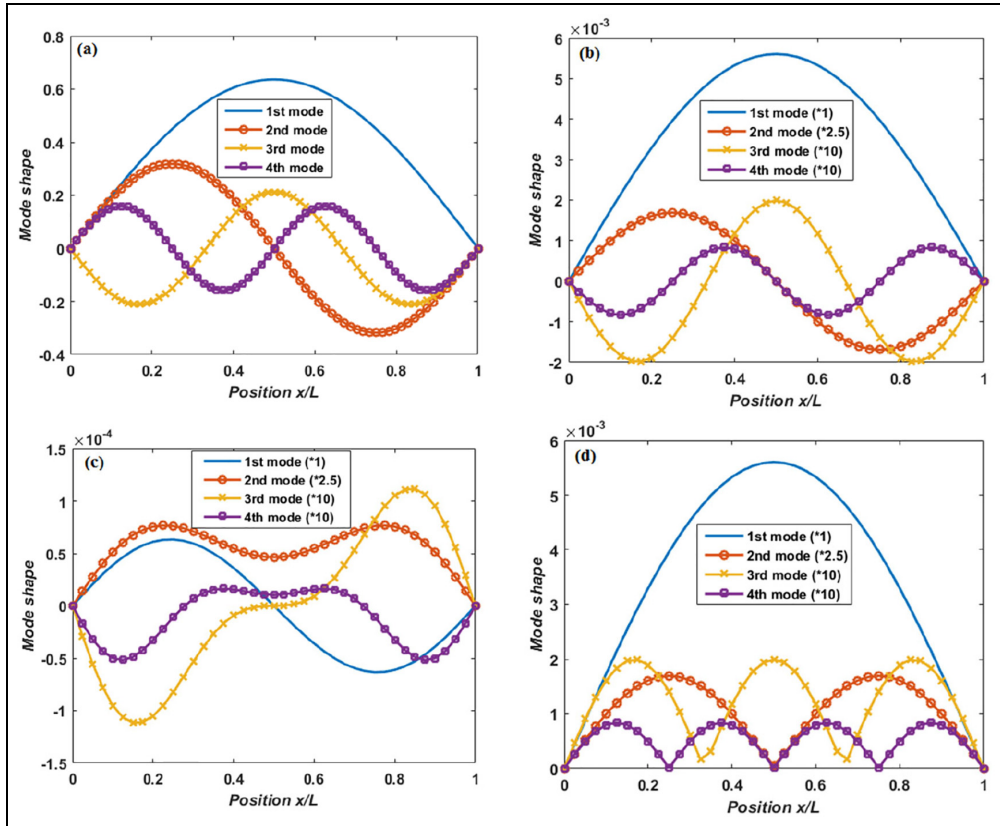


Figure 8. (a) Mode shapes for empty Pipe; (b–d) are imaginary, real, and absolute mode shapes for pipe conveying fluid at $V = 10$ m/s.

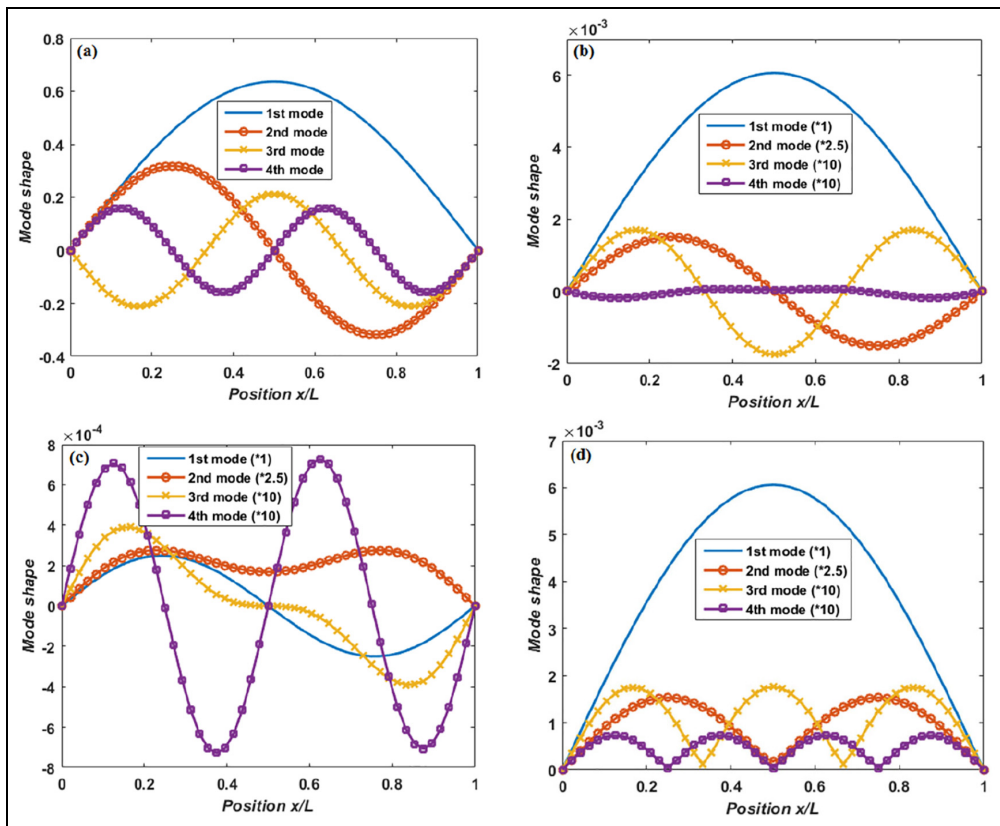


Figure 9. (a) Mode shapes for empty Pipe; (b–d) are imaginary, real, and absolute mode shapes for pipe conveying fluid at $V = 40$ m/s.

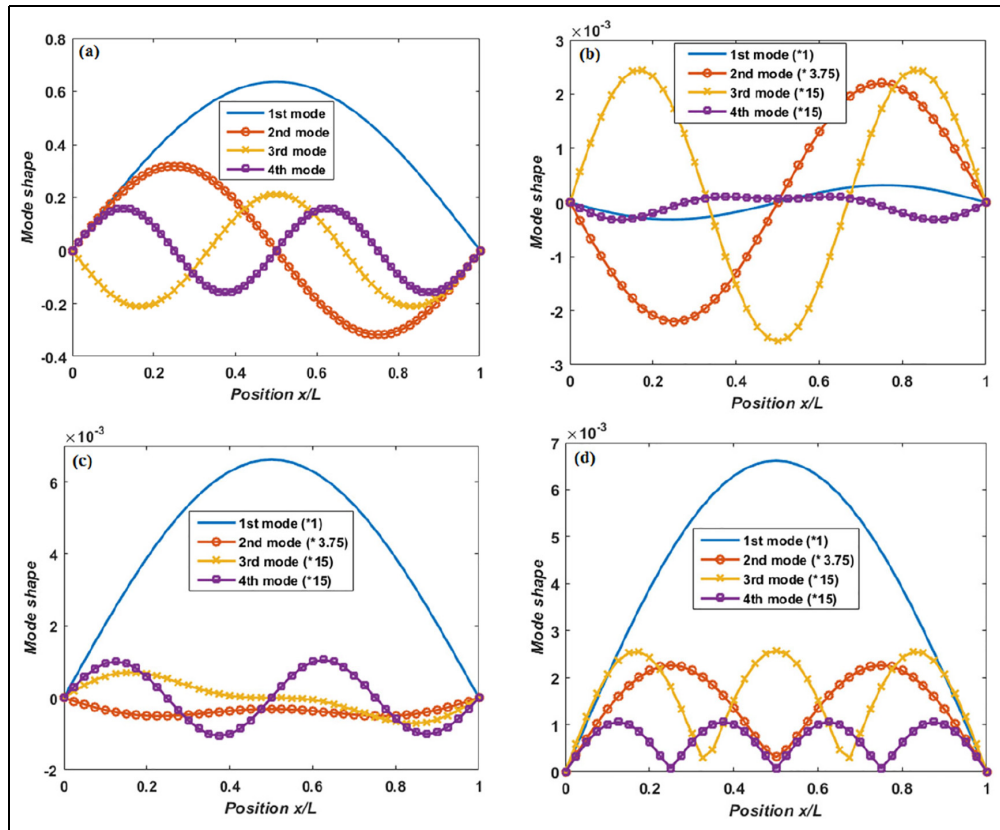


Figure 10. (a) Mode shapes for empty Pipe; (b–d) are imaginary, real, and absolute mode shapes for pipe conveying fluid at $V = 50$ m/s.

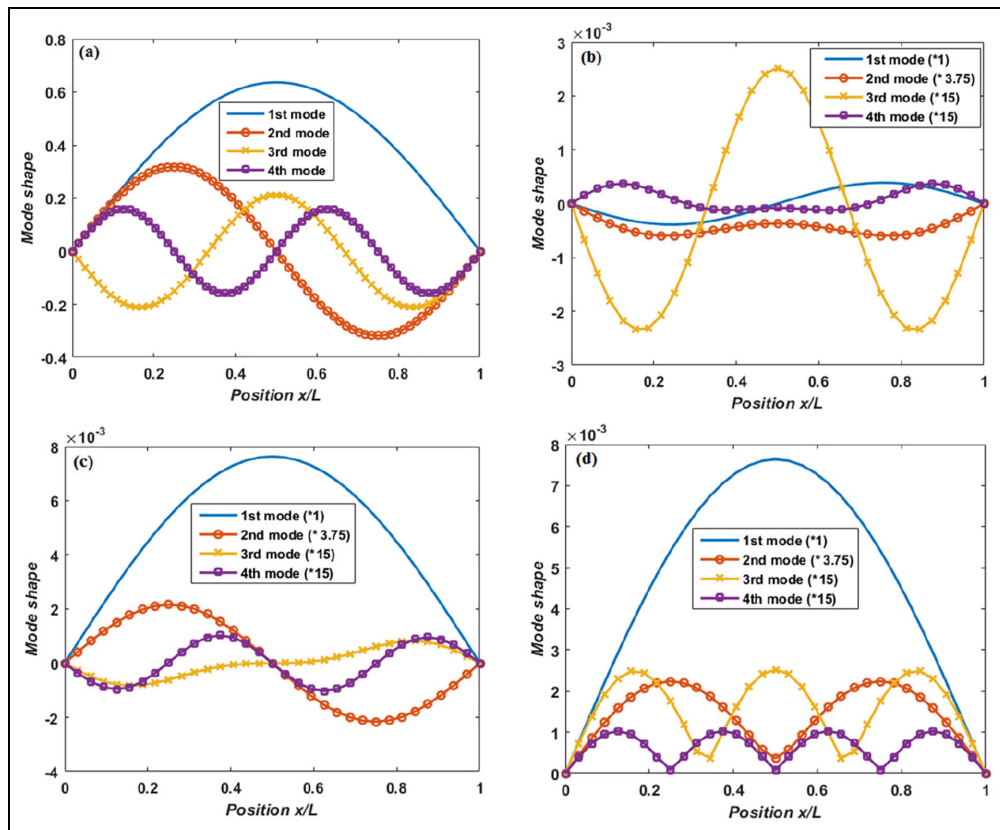


Figure 11. (a) Mode shapes for empty Pipe; (b–d) are imaginary, real, and absolute mode shapes for pipe conveying fluid at $V = 60$ m/s.

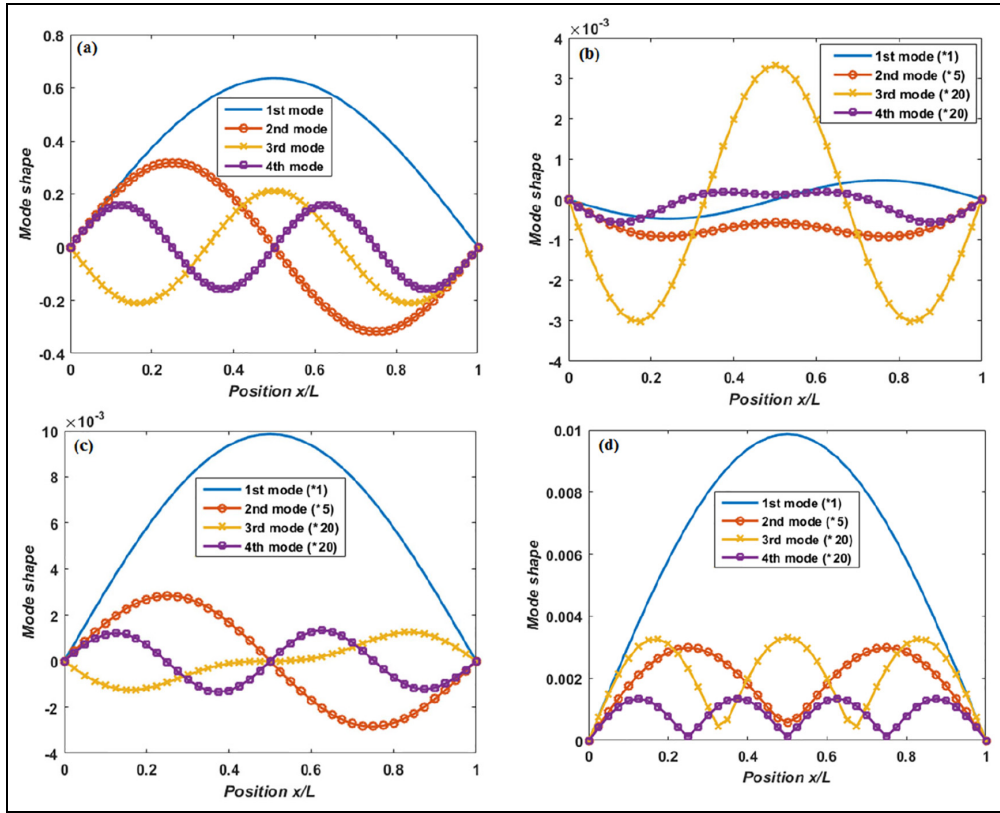


Figure 12. (a) Mode shapes for empty Pipe; (b–d) are imaginary, real, and absolute mode shapes for pipe conveying fluid at $V = 70$ m/s.

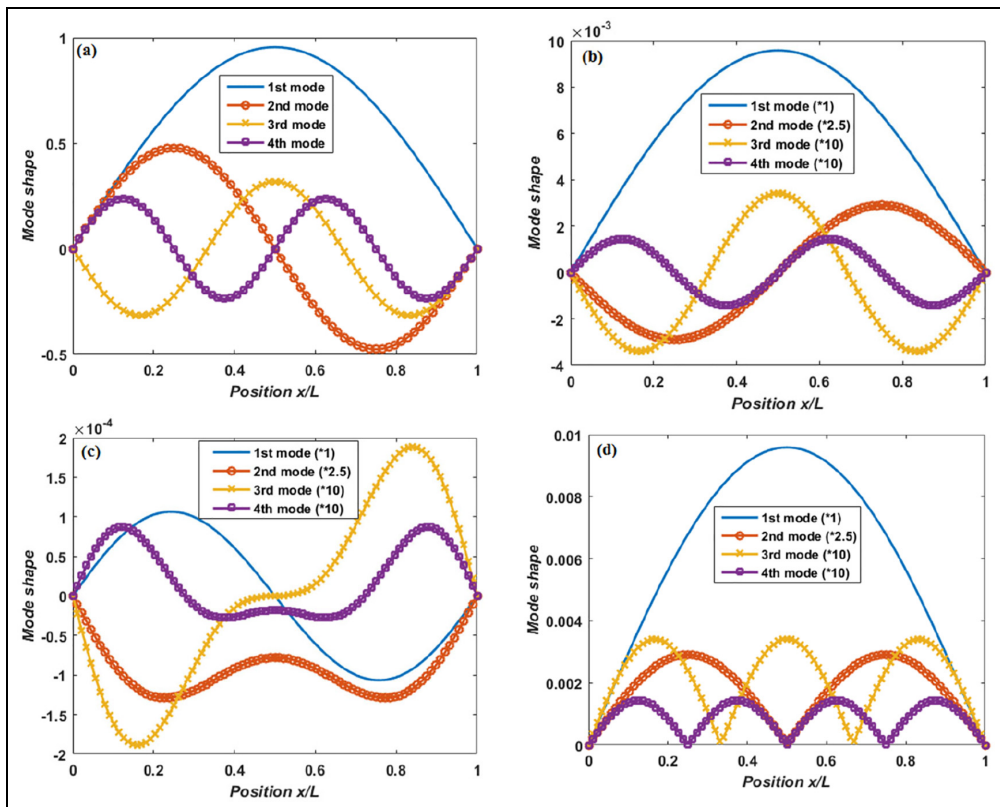


Figure 13. (a) Mode shapes for empty Pipe; (b–d) are imaginary, real, and absolute mode shapes for pipe conveying fluid at $V = 10$ m/s.

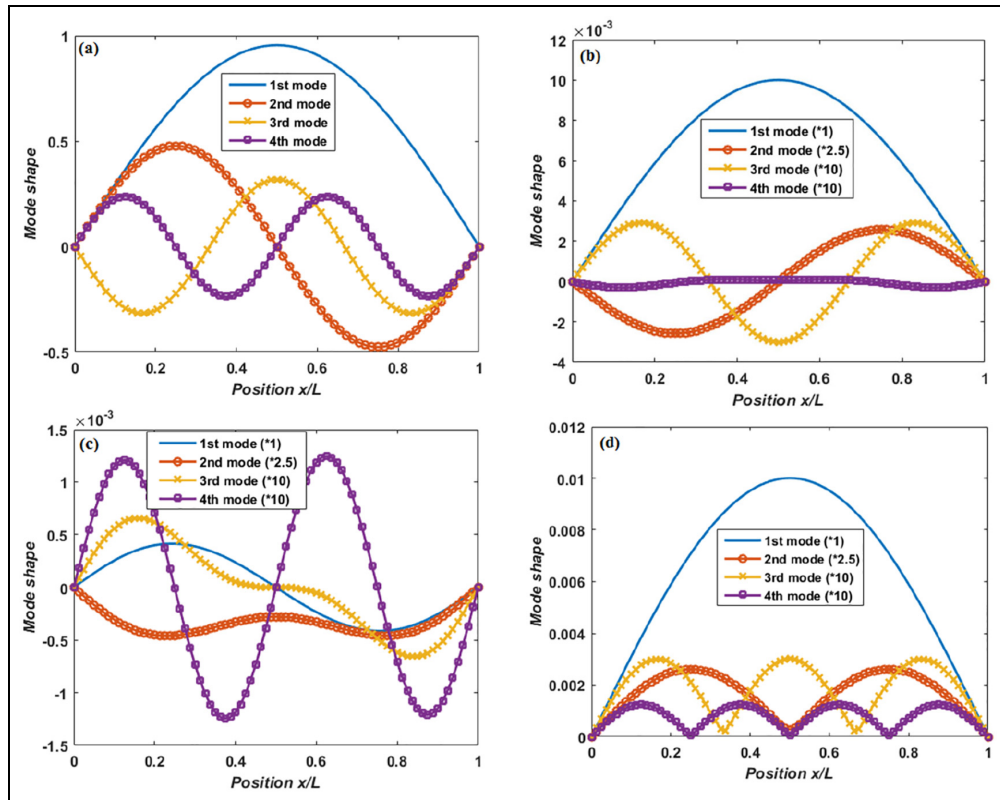


Figure 14. (a) Mode shapes for empty Pipe; (b–d) are imaginary, real, and absolute mode shapes for pipe conveying fluid at $V = 40$ m/s.

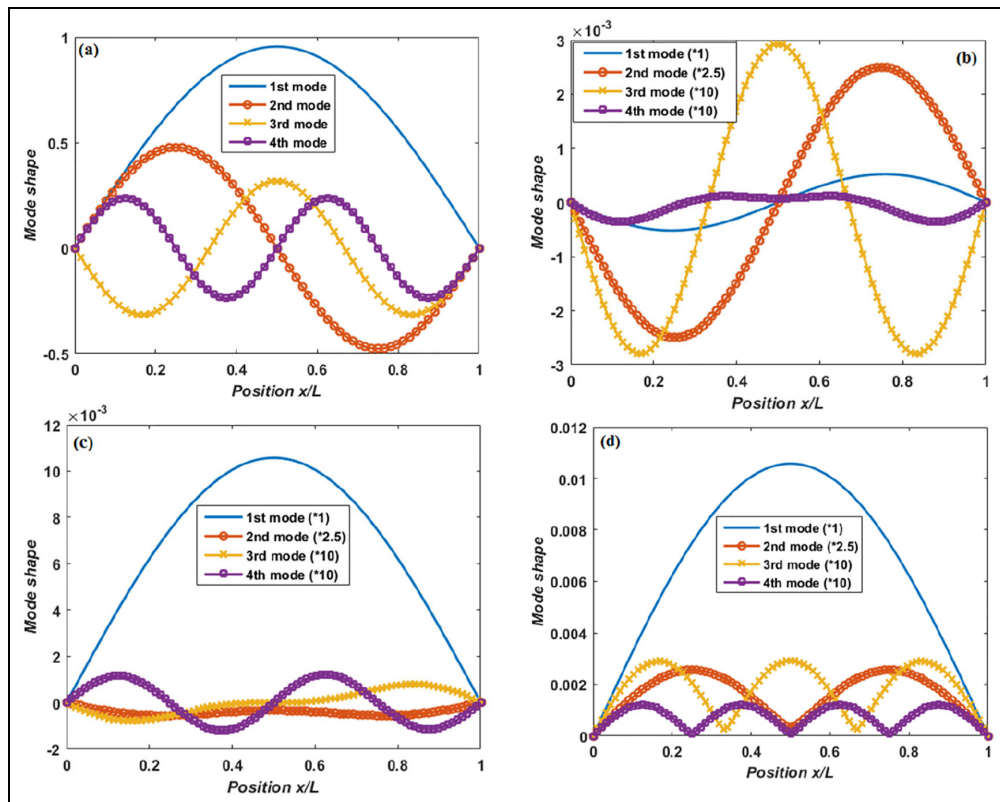


Figure 15. (a) Mode shapes for empty Pipe; (b–d) are imaginary, real, and absolute mode shapes for pipe conveying fluid at $V = 50$ m/s.

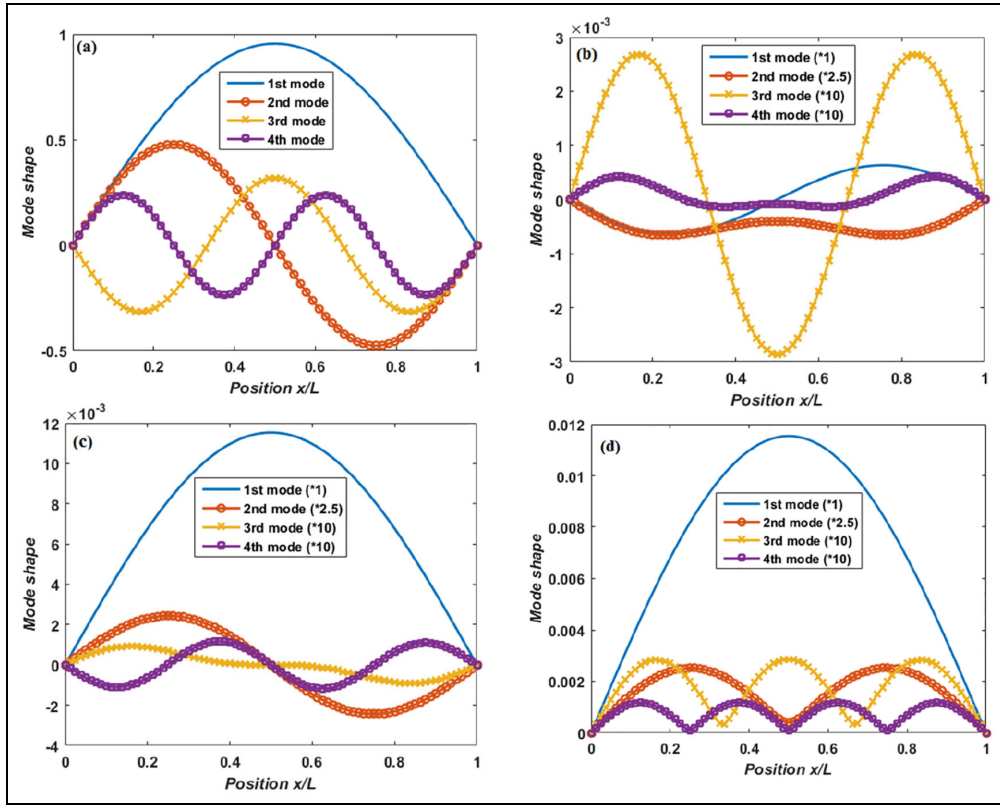


Figure 16. (a) Mode shapes for empty Pipe; (b–d) are imaginary, real, and absolute mode shapes for pipe conveying fluid at $V = 60$ m/s.

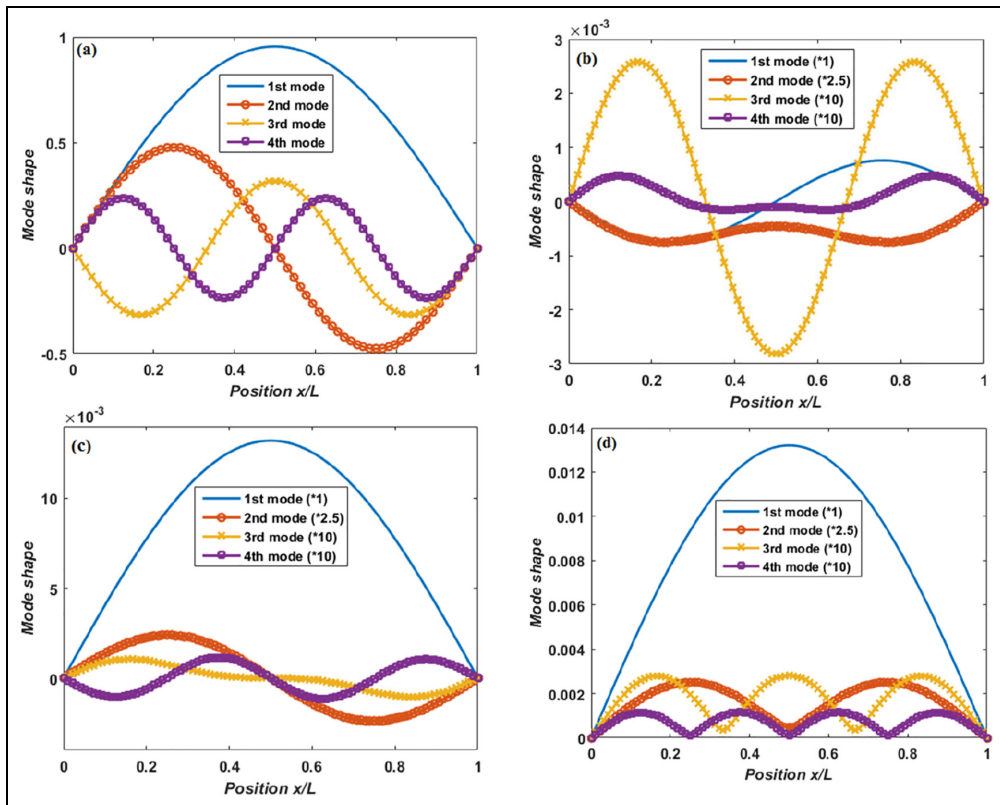


Figure 17. (a) Mode shapes for empty Pipe; (b–d) are imaginary, real, and absolute mode shapes for pipe conveying fluid at $V = 70$ m/s.

Table 2. Transition and critical velocities.

Pipe	Transition conditions			Critical conditions		
	Velocity range (m/s)	Velocity V_t^* (m/s)	First frequency (Hz) for V_t	Velocity range (m/s)	Velocity V_c^* (m/s)	First frequency (Hz) for V_c
P_1	64–65	64.53	23.7233	140–141	140.08	0
P_2	42–43	42.77	15.0382	84–85	84.09	0
P_3	44–45	44.73	13.5749	97–98	97.30	0

* Velocity with two decimal points.

absolute of the eigenvectors displayed similar mode shapes in the positive side but the real part of eigenvectors produced wrong mode shapes which cannot be used for further analysis. However, one can observe that as velocity increases, the real part of eigenvectors gives the needed mode shapes, absolute of eigenvectors continues displaying the mode shapes in the positive side while the mode shapes from imaginary part are no longer depict acceptable mode shapes.

Furthermore, it can be observed from these figures that among the three methods examined for obtaining mode shapes from the complex eigenvectors, mode shapes from either absolute or imaginary part of eigenvectors can be used to study fluid pipe displacement, failure, and other analyses at lower velocities. Conversely, at higher velocities, the mode shapes from absolute or real part of eigenvectors can be employed for fluid pipe displacement, failure, and other analyses. It becomes necessary to point out that the mode shapes obtained from absolute eigenvectors that is consistent at any velocity can be modified to look like Figure 2 by changing the signs of the required areas. Thus, instead of employing the mode shapes shown in Figure 2 that are not correct mode shapes for the pipe conveying fluid for failure and further analyses, AMSs obtained from any of these methods can be utilized.

In addition, the very significant observation was observed when acceptable AMSs for P_1 , P_2 , and P_3 abruptly shifted from imaginary part to real part of complex eigenvectors as velocity increases. It was noticed further that around this phenomenon, one or more of acceptable AMSs are presented by imaginary part while the rest are produced by real part of complex eigenvectors. This abrupt shift occurred between velocities of 60–70 m/s (see Figures 4 and 5) for P_1 , between 40 and 50 m/s (see Figures 9 and 10) for P_2 , and between 40 and 50 m/s (see Figures 14 and 15) for P_3 respectively. Further examinations around these velocities revealed that the transition of the acceptable AMSs from imaginary part to real part of complex eigenvectors commenced at velocity greater than 64, 42, and 44 m/s in that order for P_1 , P_2 , and P_3 . Interestingly, velocity of 64 m/s is closer to V_h of P_1 , 42 m/s is closer to V_h of P_2 while 44 m/s is also closer to V_h of P_3 .

Where V_h is the half of the critical velocity V_c and V_c is the velocity at which fluid pipe will fracture or fail. The details can be found in Table 2. If this table is looked into critically, it will be observed that the transition velocity V_t for each pipe is not far from the half of its V_c . The V_t is the velocity at which first mode loses shape in the imaginary part of the complex eigenvectors and appears fully in the real part of complex eigenvectors. Although, four modes were considered in this study but V_t is related to only first mode because it will occur first among all modes, it is the most destructive mode, and it is also most important in the structural dynamic analysis.

Furthermore, it can also be noticed from these figures that as velocity is closer to the transition velocity, the mode shapes obtained from the imaginary part of complex eigenvectors begin to lose their forms one after the other while reverse was the case regarding the mode shapes obtained from the real part. Hence, different from what was reported in literature, it can be inferred that neither only imaginary part nor only real part of complex eigenvectors is sufficient to obtain acceptable mode shapes of pipes conveying fluid at different velocities.

Further, another pipe P_4 was utilized to investigate the effect of length on AMSs. This pipe has the same properties as P_1 but its D_i , D_o , and L are 0.292, 0.324, and 32 m respectively. It is first frequency when it was undamped is 1.4112 Hz. When this pipe becomes fluid pipe at different velocities, it was observed that mode shapes and V_t behaved like those in the previous pipes.

Isotropic pipes

The observations under composite pipes extended this investigation to isotropic pipes and as a result, the model was modified to be able to handle isotropic pipes. The pipes P_5 and P_6 considered are defined in Table 3. The modified model was validated with empty P_5 and P_6 and the first natural frequency for each pipe was obtained to be 39.6296 and 0.8465 Hz. To validate the model further, the first frequency of P_6 at 0 m/s was determined and the result obtained (0.6955 Hz) is the same as in Bao-hui et al.³³ This shows the accuracy of

Table 3. Isotropic pipes properties.

Property	Pipe P_5	Pipe P_6 ³³
D_o	0.1282 m	0.324 m
D_i	0.1256 m	0.292 m
Length of pipe, L	3.00 m	32.00 m
Modulus of elasticity, E	210 GPa	210 GPa
Poisson ratio, ν	0.3	0.3
Density, ρ	8200 kg/m ³	8200 kg/m ³

the model. The mode shapes for the first four frequencies of these pipes when they were empty are as shown in Figure 18 and it can be observed that they are also agreed with mode shapes of pinned-pinned structures.

Now, as it was done under composite pipes, each of these pipes was then examined one after the other as the pipe conveying fluid at five different velocities that are less than each pipe critical velocity V_c . The AMSs obtained for these pipes conveying fluid at different velocities are compared with their mode shapes (in Figure 18) when they were empty pipes. The results obtained are as presented in Figures 19 to 23 for P_5 , and Figures 24–28 for P_6 respectively where “(a)” in Figures 19 to 23 is the same as Figure 18(a) and “(a)” in Figures 24 to 28 is the same as Figure 18(b). The same things observed in figures for composite pipes were also observed in figures for isotropic pipes. The details can be found in Table 4. It will be noticed in this table that the transition velocity V_t for P_5 is not far from its V_h as in Table 2 unlike that of P_6 that is away from V_h but it is closer to V_h when compare to V_c .

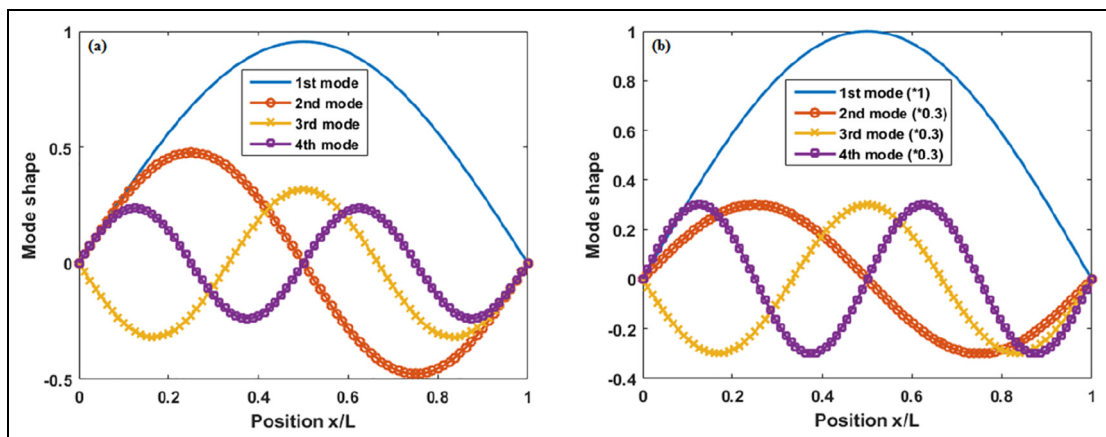
Moreover, in all the six pipes considered, it was observed that the AMSs needed for pipe failure analysis can be obtained as follows: imaginary part of complex mode shapes will give AMSs at lower fluid velocity, real part of complex mode shapes will give AMSs at higher fluid velocity while both imaginary and real parts are required to obtain AMSs around transition velocities.

Pipes failure analysis

The mode shapes obtained under different pipes are needed for successful failure analysis based on the velocity of the fluid in the pipe under consideration. It should be noted that all the pipes that have been considered above are healthy pipes and AMSs obtained at different velocities depict the actual shapes of such mode shapes. However, these mode shapes will not have the shapes of actual mode shapes once the integrity of any of these pipes (see Figure 29) is compromised. The pipe defect can grow in radial or longitudinal direction or both as time passes by. Thus, if the cross-sections of the region with and region without defect in Figure 29 are expanded they can be presented as shown in Figure 30. In this figure, t_o , t_n , t_d , and l_d are original pipe thickness, thickness of the region not affected by defect, thickness of defected region, and length of the defect along pipe span respectively. The pipe defect could form any shape but in this work, the defect is assumed to be circular for simplicity as shown in Figure 30(c). The mass and stiffness of the region with defect will continue to change as defect shape increases while the volume of the fluid at the region will increase.

As a case study, pipe P_2 was considered as a pipe with defect wherein $t_d = t_o/2$ m; $l_d = L/10$ m; and $l_c = L/4, L/2$, and $4L/5$ m where l_c is the defect location along the pipe span. The frequencies of this defected pipe as an empty and as a pipe conveying fluid are presented in Tables 5 and 6 in that order. The effects of the defect on the pipe can be seen in both tables and these will continue as the defect grows till the failure eventually occurs.

Furthermore, the presence of the defect in the pipe can be noticed in the pipe mode shapes in which they will be deformed unlike when the pipe is healthy. This deformation will appear around the location where defect is present along the pipe span. Figures 31 to 33

**Figure 18.** Different pipes mode shapes for the first four frequencies: (a) P_5 and (b) P_6 .

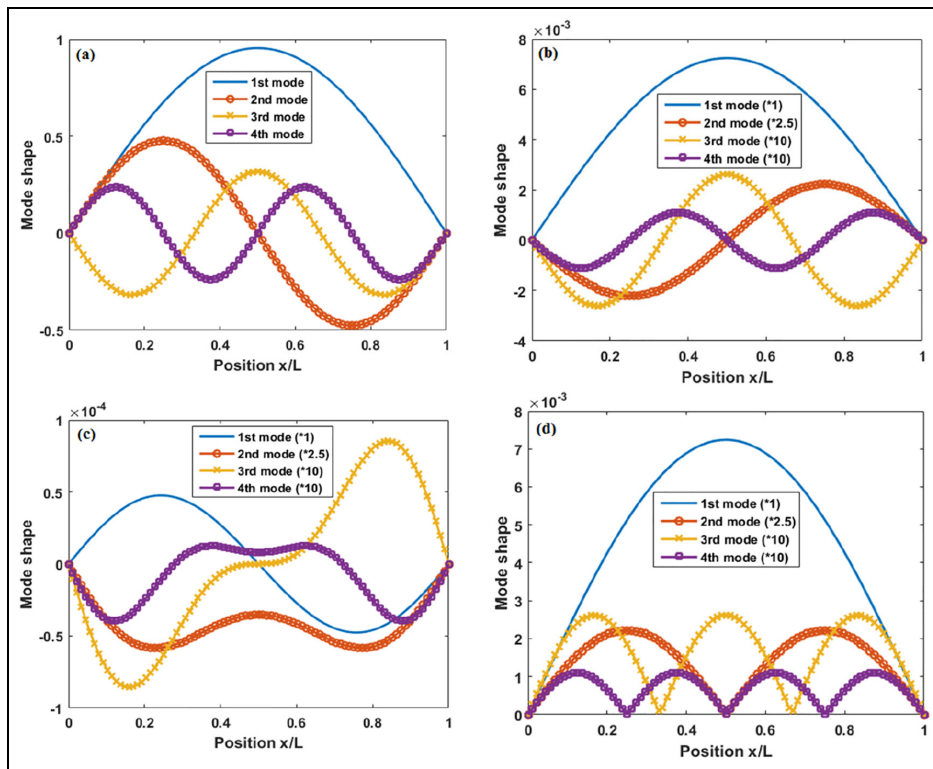


Figure 19. (a) Mode shapes for empty Pipe; (b–d) are imaginary, real, and absolute mode shapes for pipe conveying fluid at $V = 10$ m/s.

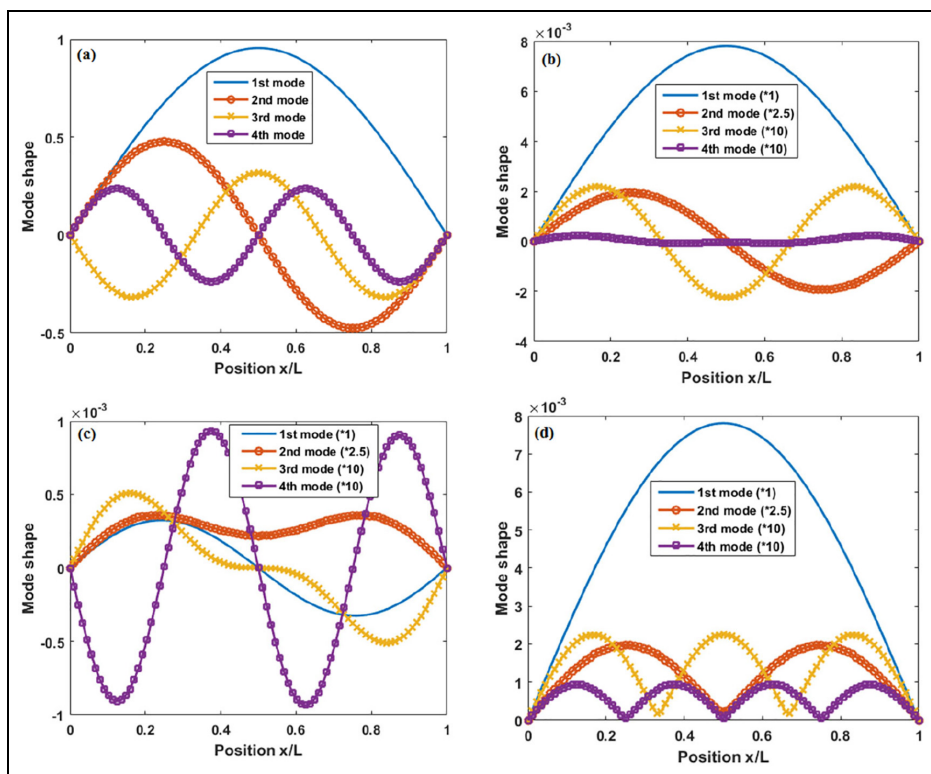


Figure 20. (a) Mode shapes for empty Pipe; (b–d) are imaginary, real, and absolute mode shapes for pipe conveying fluid at $V = 70$ m/s.

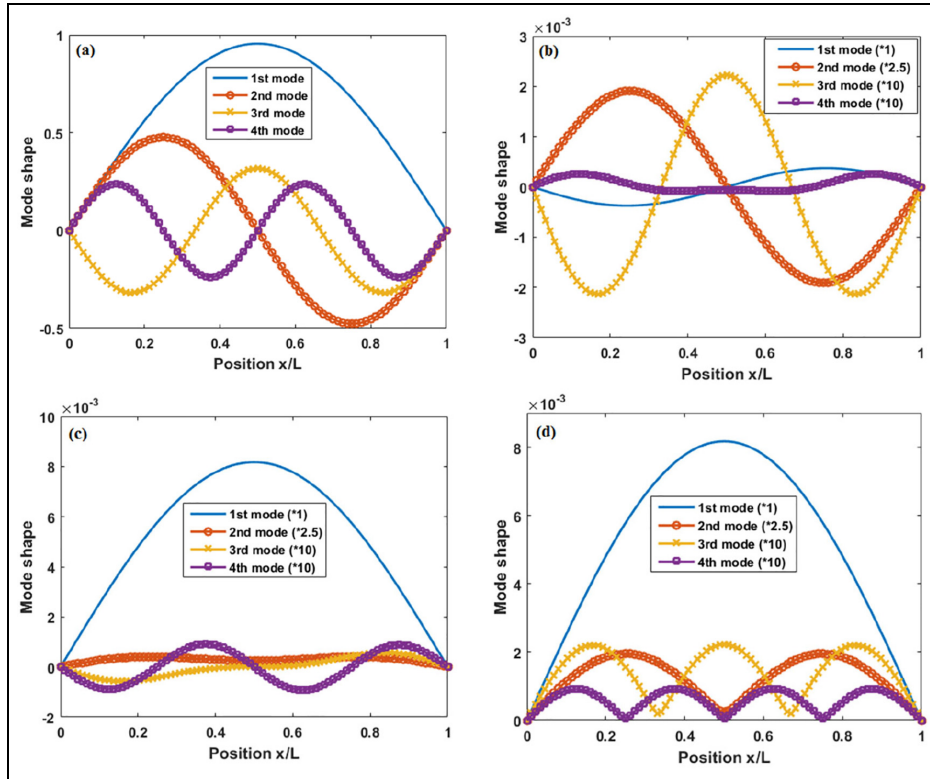


Figure 21. (a) Mode shapes for empty Pipe; (b–d) are imaginary, real, and absolute mode shapes for pipe conveying fluid at $V = 80$ m/s.

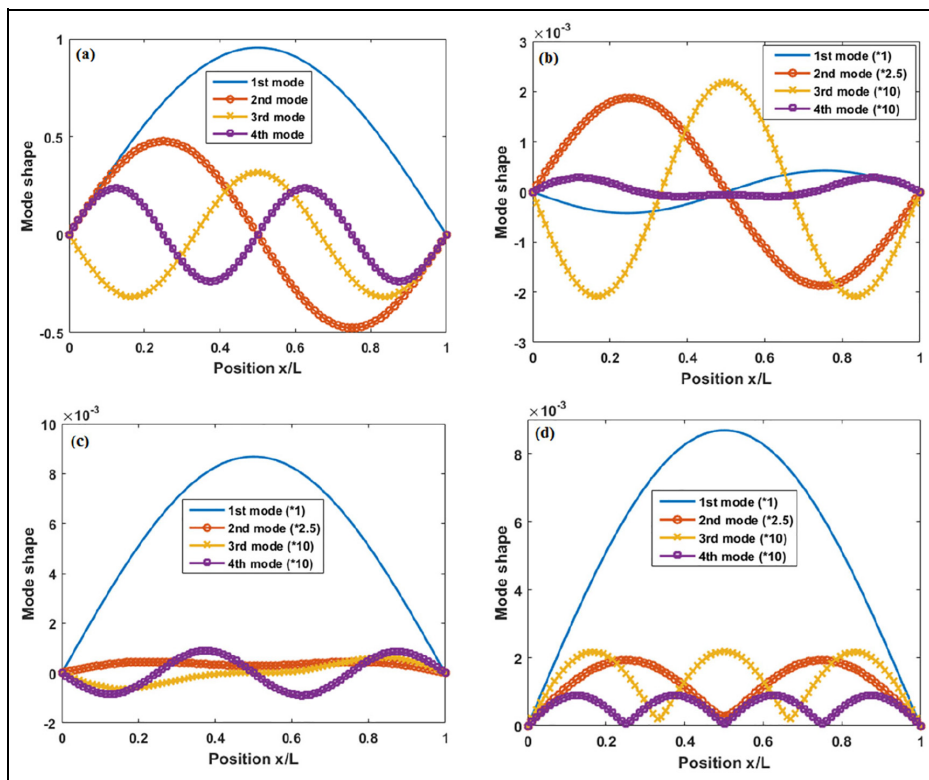


Figure 22. (a) Mode shapes for empty Pipe; (b–d) are imaginary, real, and absolute mode shapes for pipe conveying fluid at $V = 90$ m/s.

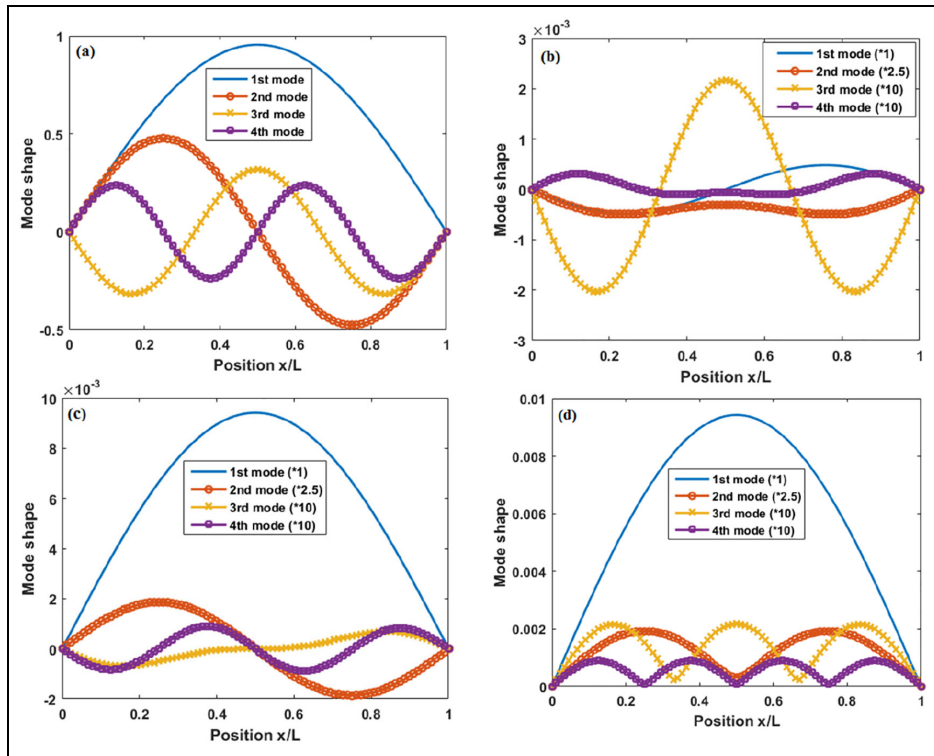


Figure 23. (a) Mode shapes for empty Pipe; (b–d) are imaginary, real, and absolute mode shapes for pipe conveying fluid at $V = 100$ m/s.

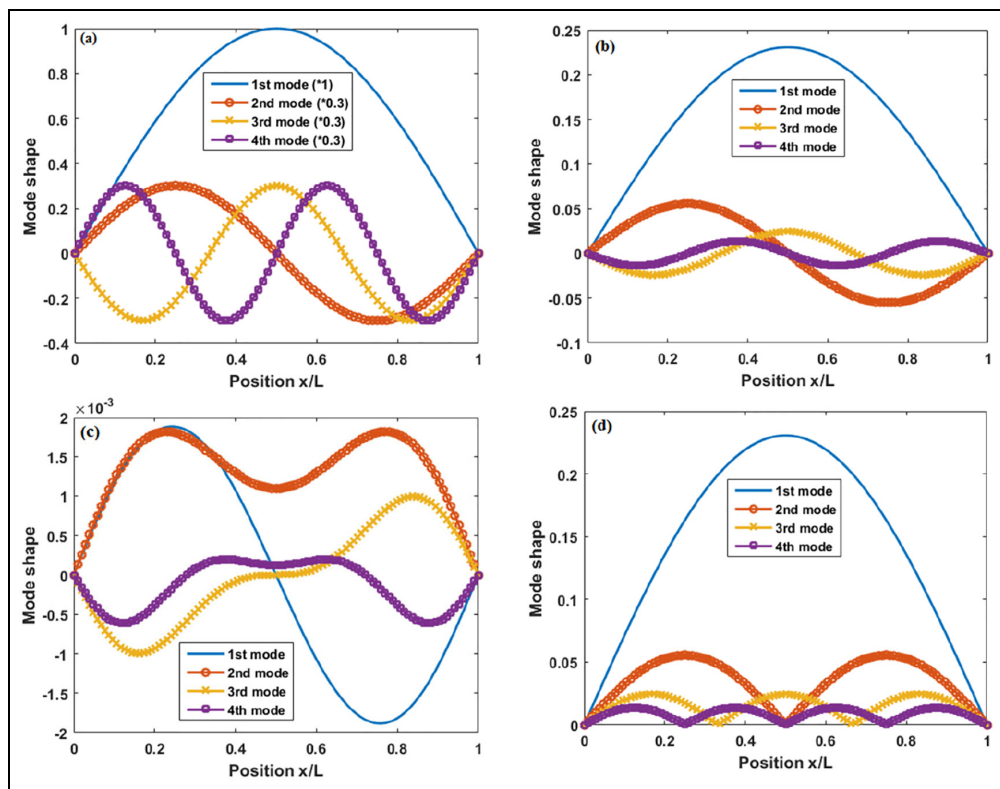


Figure 24. (a) Mode shapes for empty Pipe; (b–d) are imaginary, real, and absolute mode shapes for pipe conveying fluid at $V = 10$ m/s.

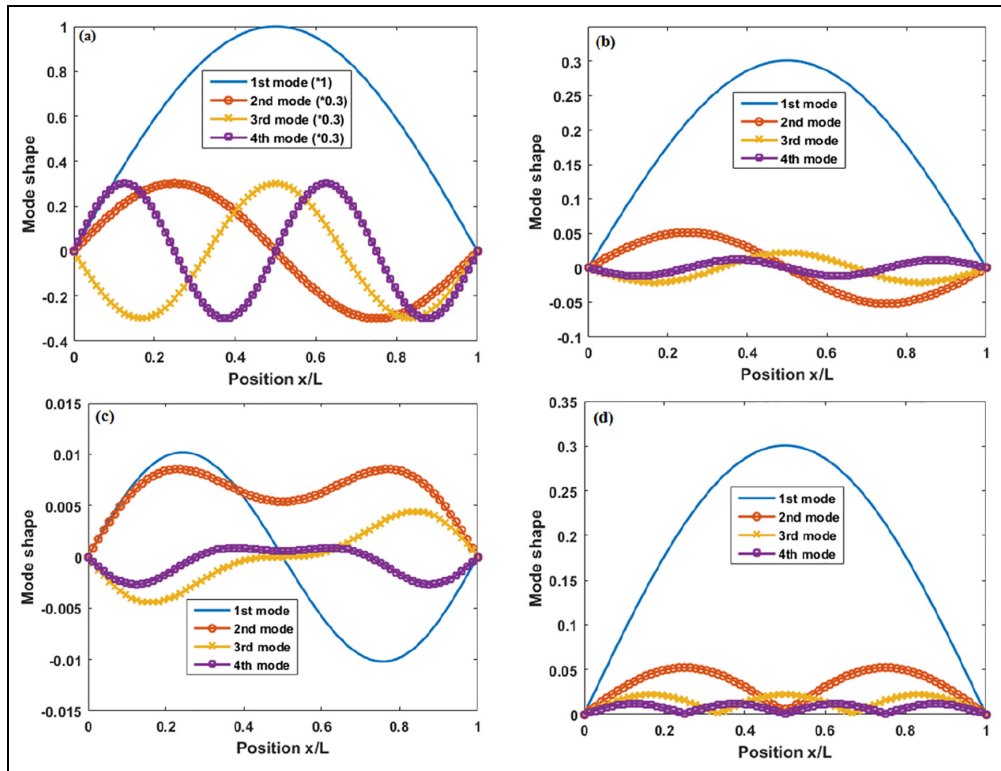


Figure 25. (a) Mode shapes for empty Pipe; (b–d) are imaginary, real, and absolute mode shapes for pipe conveying fluid at $V = 50$ m/s.

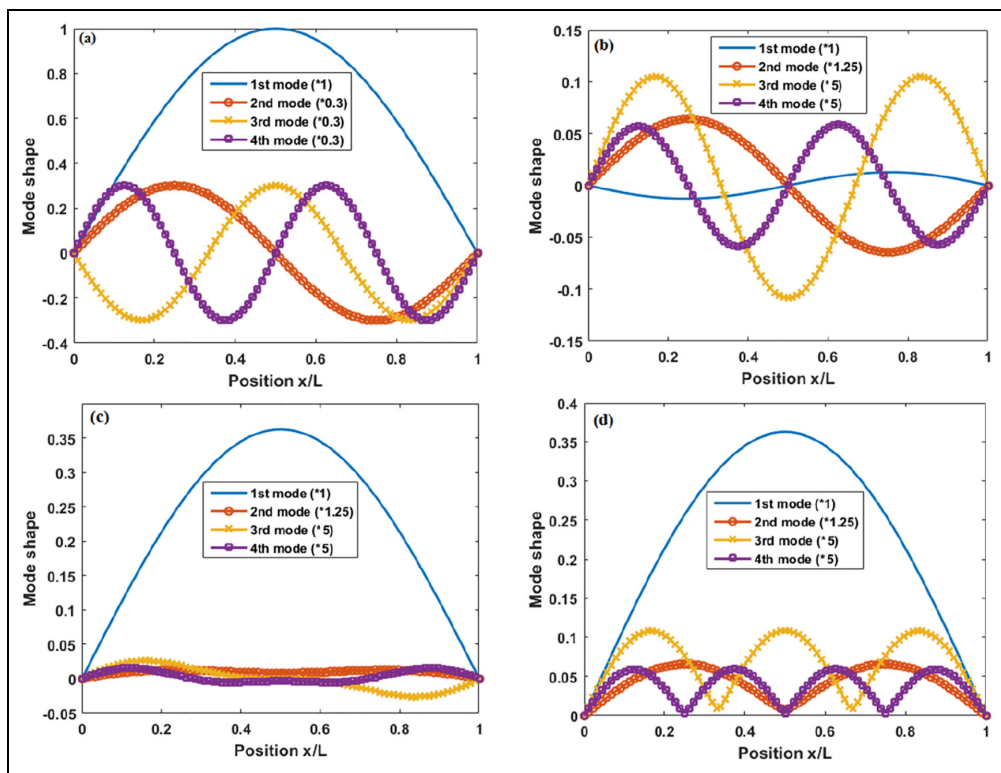


Figure 26. (a) Mode shapes for empty Pipe; (b–d) are imaginary, real, and absolute mode shapes for pipe conveying fluid at $V = 60$ m/s.

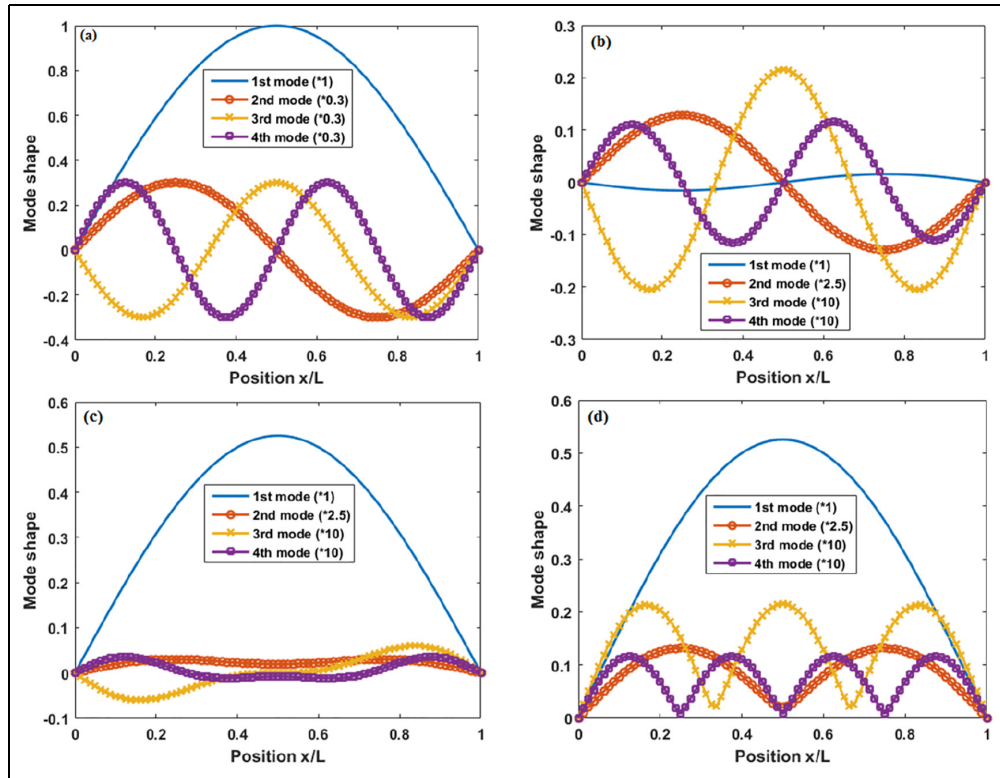


Figure 27. (a) Mode shapes for empty Pipe; (b–d) are imaginary, real, and absolute mode shapes for pipe conveying fluid at $V = 70$ m/s.

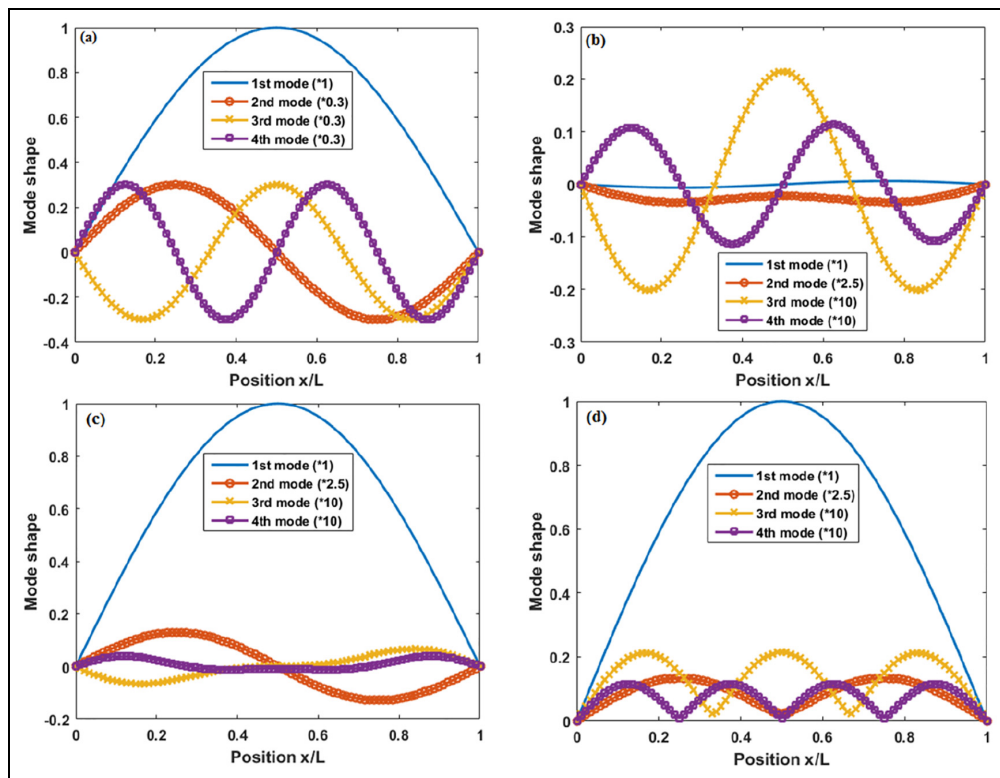


Figure 28. (a) Mode shapes for empty Pipe; (b–d) are imaginary, real, and absolute mode shapes for pipe conveying fluid at $V = 78$ m/s.

Table 4. Isotropic pipes transition and critical velocities.

Pipe	Transition conditions			Critical conditions		
	Velocity range (m/s)	Velocity V_t^* (m/s)	First frequency (Hz) at V_t	Velocity range (m/s)	Velocity V_c^* (m/s)	First frequency (Hz) at V_c
P_5	73–74	73.64	17.5938	146–147	146.20	0
P_6	50–51	50.24	0.5263	78–79	78.30	0

* Velocity with two decimal points.

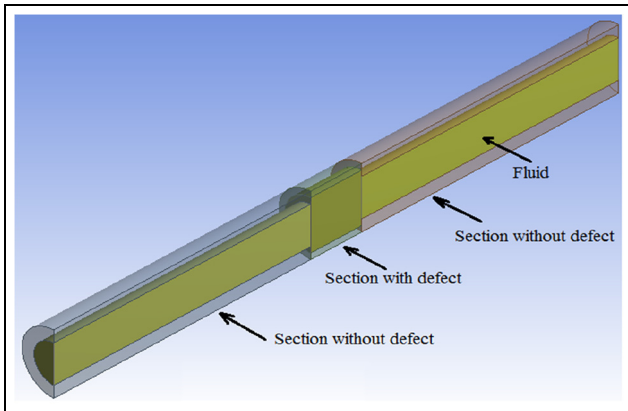


Figure 29. Pipe with internal defect.

show the new deformed mode shapes of Figure 8(b) and (d) while Figures 34 to 36 display the new deformed mode shapes of Figure 11(b) to (d) for pipe P_2 when its integrity has been compromised with internal defect as shown in Figure 29. This defect may occur due to erosion, chemical attack or other factors at different locations along the pipe span. Once this occurred, the pipes can be marked for maintenance or replacement to prevent total failure and its consequences.

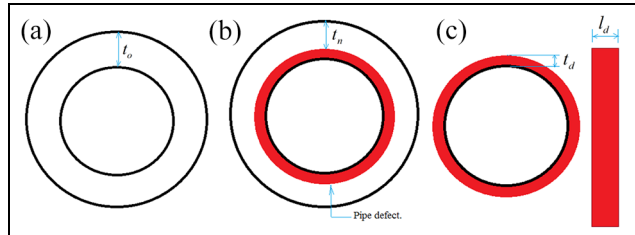


Figure 30. Cross-sections of different regions of pipe with internal defect: (a) cross-section of region without defect, (b) cross-section of the region with defect, and (c) pipe defect and its width.

Table 5. Frequency of empty pipe P_2 with defect at different locations.

S/N	Frequency of healthy pipe P_2 (Hz)	Frequency of pipe P_2 with defect (Hz)		
		$l_c = L/4 m$	$l_c = L/2 m$	$l_c = 4L/5 m$
1	33.4224	32.9600	32.5790	33.0873
2	133.6896	131.6241	133.5404	131.6785
3	300.8017	299.4132	298.8008	298.6914
4	534.7590	532.8752	532.8749	533.2888
5	835.5622	835.0721	838.5242	831.6705

Table 6. Frequency of pipe P_2 conveying fluid with defect at different locations.

Velocity (m/s)	Pipe type		Frequency (Hz)				
			f_1	f_2	f_3	f_4	f_5
0	Healthy pipe		17.7944	71.1778	160.1500	284.7113	444.8621
	Pipe with defect	$l_c = L/4 m$	17.1242	66.6366	155.3530	281.9764	430.8833
		$l_c = L/2 m$	16.5461	70.9949	150.9925	281.9795	424.9021
10	Pipe with defect	$l_c = 4L/5 m$	17.3191	66.8735	152.0967	278.3392	438.5106
		Healthy pipe	17.6508	71.0684	160.0501	284.6162	444.7698
		Pipe with defect	$l_c = L/4 m$	16.9739	66.5206	155.2505	281.8803
	Pipe with defect	$l_c = L/2 m$	16.3911	70.8842	150.8905	281.8838	424.8072
		$l_c = 4L/5 m$	17.1709	66.7569	151.9919	278.2423	438.4172
60	Healthy pipe		12.0034	67.1654	156.5336	281.2786	441.5369
	Pipe with defect	$l_c = L/4 m$	10.9959	62.3643	151.6402	278.5070	427.4814
		$l_c = L/2 m$	10.0818	66.9386	147.2962	278.5277	421.4819
		$l_c = 4L/5 m$	11.3155	62.5753	148.3008	274.8427	435.1400

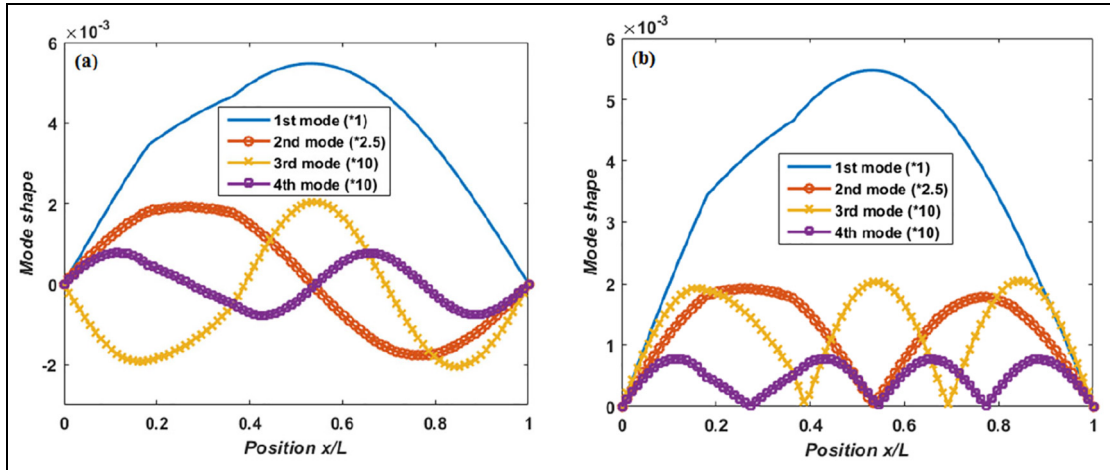


Figure 31. (a, b) Imaginary and absolute mode shapes for pipe with internal defect at $l_c = L/4$ and conveying fluid at $V = 10$ m/s.

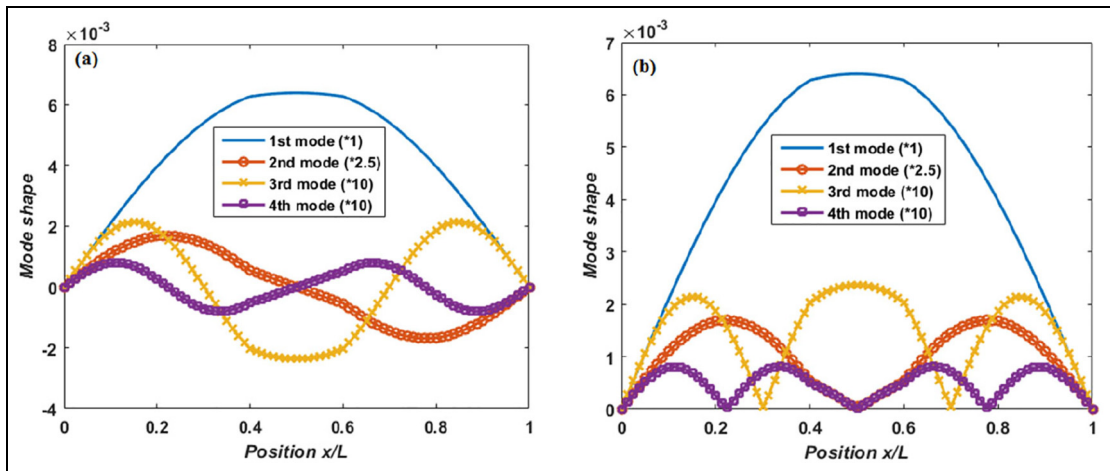


Figure 32. (a, b) Imaginary and absolute mode shapes for pipe with internal defect at $l_c = L/2$ and conveying fluid at $V = 10$ m/s.

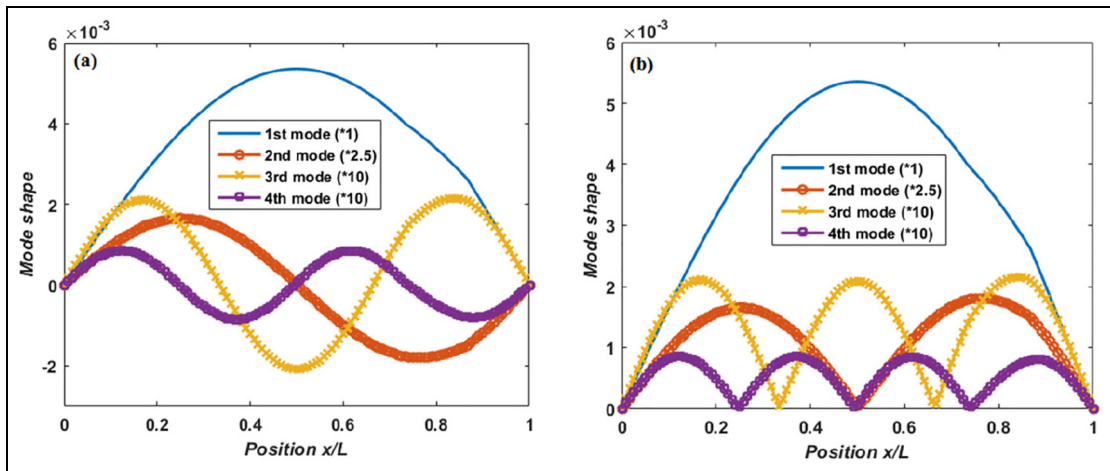


Figure 33. (a, b) Imaginary and absolute mode shapes for pipe with internal defect at $l_c = 4L/5$ and conveying fluid at $V = 10$ m/s.

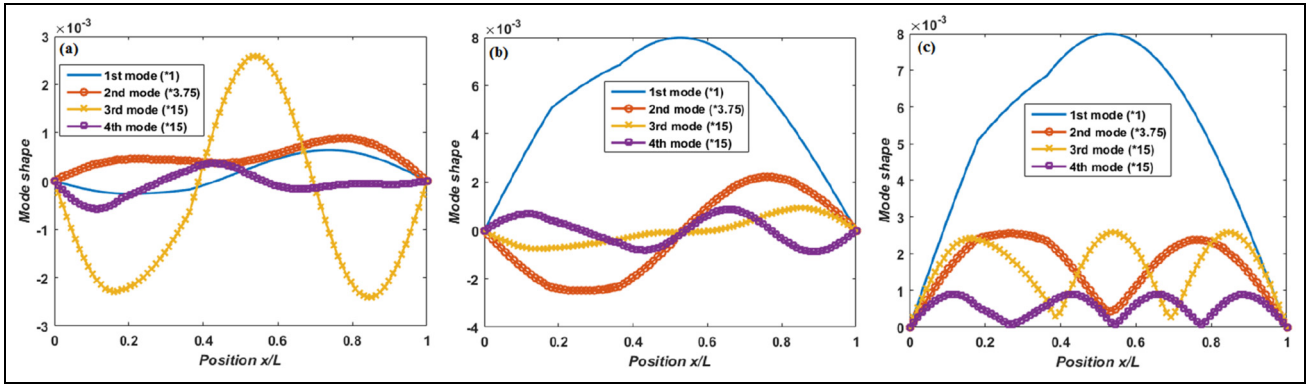


Figure 34. (a–c) Imaginary, real, and absolute mode shapes for pipe with internal defect at $l_c=L/4$ and conveying fluid at $V=60$ m/s.

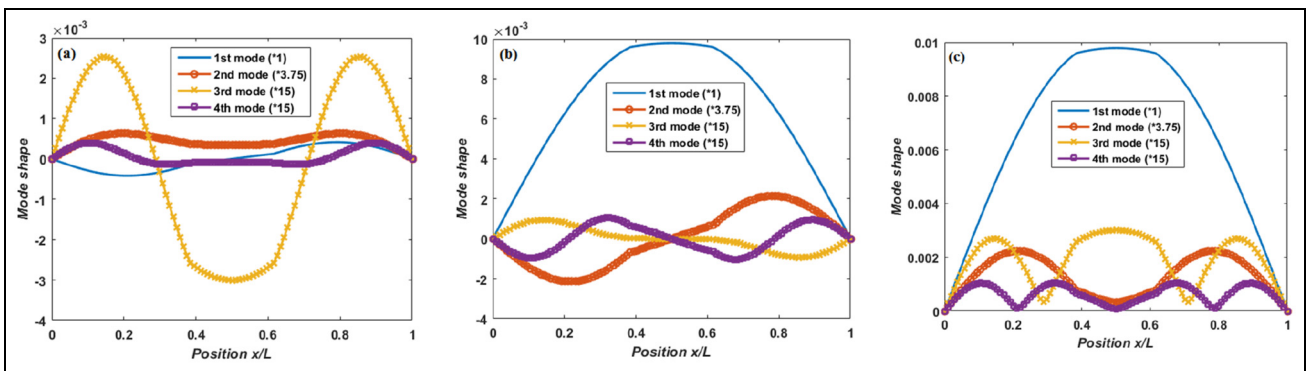


Figure 35. (a–c) are imaginary, real, and absolute mode shapes for pipe with internal defect at $l_c = L/2$ and conveying fluid at $V = 60$ m/s.

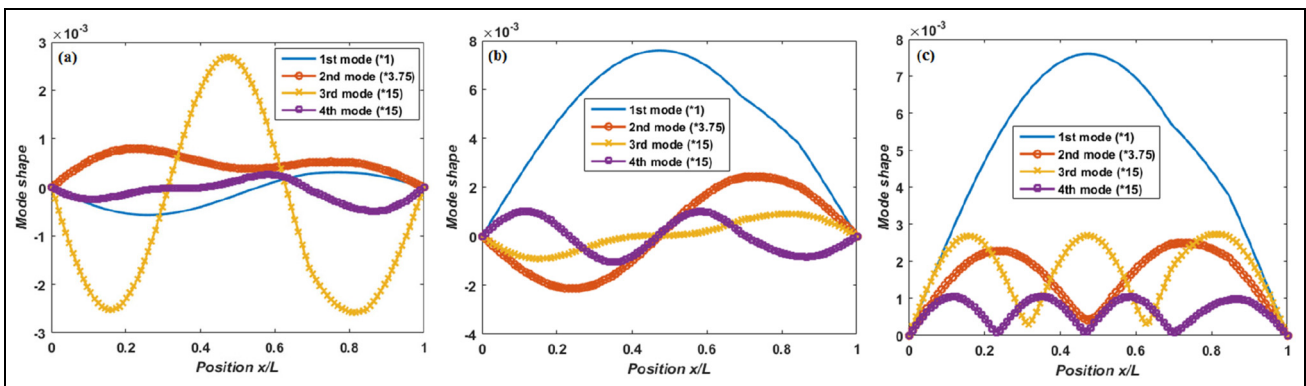


Figure 36. (a–c) Imaginary, real, and absolute mode shapes for pipe with internal defect at $l_c = 4L/5$ and conveying fluid at $V = 60$ m/s.

Conclusions

Mode shapes are crucial in dynamic analysis of the structures. Three different techniques for obtaining AMSs of pipes with flowing fluid and their characteristics as the fluid velocity increases were presented, and their application in the pipe failure analysis were

investigated in this work. It was observed that when there is substantial compromise in the pipe integrity due to erosion, chemicals in the fluid, corrosion, and so on; the mode shapes will be deformed. The real deformation that will indicate that the pipe has been compromised will appear in one or more of the three methods presented based on the fluid velocity. In this

study, at lower velocities this actual deformation was noticed in the mode shapes from imaginary part or absolute of complex eigenvectors while it appeared in the mode shapes from the real part or absolute of complex eigenvectors at higher velocities. On the contrary, the deformation emerged in the mode shapes from all techniques around transition velocities. Once the actual deformation is noticed, the pipe under consideration can be marked as the pipe that will fail sooner or later if necessary maintenance is not done.

Hence, the findings in this study support the initiative that AMSs can be employed to assess or monitor fluid pipe integrity in order to reduce revenue loss, leakage, plant shutdown time, and prevent catastrophic failures.


Declaration of conflicting interests

The author(s) declared no potential conflicts of interest with respect to the research, authorship, and/or publication of this article.

Funding

The author(s) received no financial support for the research, authorship, and/or publication of this article.

ORCID iD

Wasiu Adeyemi Oke  <https://orcid.org/0000-0003-0027-4370>

References

- Bhardwaj U, Teixeira AP and Soares CG. Reliability assessment of a subsea pipe-in-pipe system for major failure modes. *Int J Press Vessel Piping* 2020; 188: 104177.
- Chu Q, Zhang M, Li J, et al. Failure analysis of a steam pipe weld used in power generation plant. *Eng Fail Anal* 2014; 44: 363–370.
- Majid ZA, Mohsin R and Yusof MZ. Experimental and computational failure analysis of natural gas pipe. *Eng Fail Anal* 2012; 19: 32–42.
- Tang K, Parsons DJ and Jude S. Comparison of automatic and guided learning for Bayesian networks to analyse pipe failures in the water distribution system. *Reliab Eng Syst Saf* 2019; 186: 24–36.
- Robles-Velasco A, Cortés P, Muñuzuri J, et al. Prediction of pipe failures in water supply networks using logistic regression and support vector classification. *Reliab Eng Syst Saf* 2020; 196: 106754.
- Ashrafizadeh H, Karimi M and Ashrafizadeh F. Failure analysis of a high pressure natural gas pipe under split tee by computer simulations and metallurgical assessment. *Eng Fail Anal* 2013; 32: 188–201.
- El-Gebeily M, Khulief Y and Ghneim A. A multiresolution approach for damage detection in fiber-reinforced polymer pipe systems. *Adv Mech Eng* 2016; 8: 1687814016668707.
- Ying W, Cuiyun J and Yanhui Z. Pipe defect detection and reconstruction based on 3D points acquired by the circular structured light vision. *Adv Mech Eng* 2013; 5: 670487.
- Rezaei H, Ryan B and Stoianov I. Pipe failure analysis and impact of dynamic hydraulic conditions in water supply networks. *Procedia Eng* 2015; 119: 253–262.
- Zhang Y, Zhao H and Lie ST. Estimation of mode shapes of beam-like structures by a moving lumped mass. *Eng Struct* 2019; 180: 654–668.
- Wu J. Computer animation of structural mode shapes. In: *2014 international conference on multimedia computing and systems (ICMCS)*, Marrakech, Morocco, 14–16 April 2014, pp.1–4.
- Thomas J, Gurusamy S, Rajanna TR, et al. Structural shape estimation by mode shapes using fiber bragg grating sensors: a genetic algorithm approach. *IEEE Sens J* 2019; 20: 2945–2952.
- Koruk H and Sanliturk KY. A novel definition for quantification of mode shape complexity. *J Sound Vib* 2013; 332: 3390–3403.
- He J and Zhou Y. A novel mode shape reconstruction method for damage diagnosis of cracked beam. *Mech Syst Signal Process* 2019; 122: 433–447.
- El-Sayed TA and El-Mongy HH. Free vibration and stability analysis of a multi-span pipe conveying fluid using exact and variational iteration methods combined with transfer matrix method. *Appl Math Model* 2019; 71: 173–193.
- Bahaadini R, Dashtbayazi MR, Hosseini M, et al. Stability analysis of composite thin-walled pipes conveying fluid. *Ocean Eng* 2018; 160: 311–323.
- Liu M, Wang Z, Zhou Z, et al. Vibration response of multi-span fluid-conveying pipe with multiple accessories under complex boundary conditions. *Eur J Mech A Solids* 2018; 72: 41–56.
- Yun-dong L and Yi-ren Y. Vibration analysis of conveying fluid pipe via He's variational iteration method. *Appl Math Model* 2017; 43: 409–420.
- Mediano-Valiente B and Garcia Planas MI. Stability analysis of a clamped-pinned pipeline conveying fluid. *WSEAS Trans Syst* 2014; 13: 54–64.
- Arjmandi SA and Lotfi V. Computing mode shapes of fluid-structure systems using subspace iteration methods. *Sci Iran* 2011; 18: 1159–1169.
- Ryu S-U, Sugiyama Y and Ryu B-J. Eigenvalue branches and modes for flutter of cantilevered pipes conveying fluid. *Comput Struct* 2002; 80: 1231–1241.
- Wang L, Dai H and Ni Q. Nonconservative pipes conveying fluid: evolution of mode shapes with increasing flow velocity. *J Vib Control* 2015; 21: 3359–3367.
- Zhou X-W, Dai H-L and Wang L. Dynamics of axially functionally graded cantilevered pipes conveying fluid. *Compos Struct* 2018; 190: 112–118.
- Sarkar A and Paidoussis MP. A cantilever conveying fluid: coherent modes versus beam modes. *Int J Non Linear Mech* 2004; 39: 467–481.
- Alfosail FK, Nayfeh AH and Younis MI. Natural frequencies and mode shapes of statically deformed inclined risers. *Int J Non Linear Mech* 2017; 94: 12–19.
- Chen Y, Chai YH, Li X, et al. An extraction of the natural frequencies and mode shapes of marine risers by the

- method of differential transformation. *Comput Struct* 2009; 87: 1384–1393.
27. Oke WA, Adeyemi OA, Bello KA, et al. Approximate mode shape for damped structures. In: Gdoutos EE (ed.) *Proceedings of the second international conference on theoretical, applied and experimental mechanics*. Cham: Springer International Publishing, 2019, pp.9–14.
 28. Oke WA and Khulief YA. Effect of internal surface damage on vibration behavior of a composite pipe conveying fluid. *Compos Struct* 2018; 194: 104–118.
 29. Bauchau OA. *Design, manufacturing and testing of high speed rotating graphite/epoxy shafts*. Cambridge, MA: Massachusetts Institute of Technology, 1981.
 30. Qatu MS and Iqbal J. Transverse vibration of a two-segment cross-ply composite shafts with a lumped mass. *Compos Struct* 2010; 92: 1126–1131.
 31. Oke WA and Khulief YA. B-spline wavelet-based finite element vibration analysis of composite pipes with internal surface defects of different geometries. *Int J Struct Stab Dyn* 2017; 17: 1750051.
 32. Oke WA and Khulief YA. Vibration analysis of composite pipes using the finite element method with B-spline wavelets. *J Mech Sci Technol* 2016; 30: 623–635. journal article.
 33. Bao-hui L, Hang-shan G, Yong-shou L, et al. Transient response analysis of multi-span pipe conveying fluid. *J Vib Control* 2013; 19: 2164–2176.